A Becker-Döring model of competitive nucleation

1999 J. Phys. A: Math. Gen. 32 8755

(http://iopscience.iop.org/0305-4470/32/49/315)

J. Phys. A: Math. Gen. **32** (1999) 8755–8784. Printed in the UK PII: S0305-4470(99)02514-7

A Becker–Döring model of competitive nucleation

Jonathan A D Wattis

Division of Theoretical Mechanics, School of Mathematical Sciences, University of Nottingham, University Park, Nottingham NG7 2RD, UK

E-mail: Jonathan.Wattis@nottingham.ac.uk

Received 10 March 1999, in final form 25 August 1999

Abstract. We introduce a modified Becker–Döring system of equations which models the nucleation of two types of cluster from the same monomer. This competitive nucleation system is then studied in the coagulation-dominated asymptotic regime where a succession of timescales is identified through which the system passes, and in which the cluster distribution profile is described. The system is then subjected to a coarse-grain rescaling leading to a low-dimensional system of equations for macroscopically observable quantities. This system is also solved in the coagulation-dominated regime. Examples of the full system and the reduced system are solved numerically to show the similarities in the behaviour exhibited by their respective solutions. This study has applications to experiments involving crystallization where various morphologies of growing crystals are observed, and to protein crystallization, where gels and/or amorphous material precipitate out of solution simultaneously with crystals. We highlight how some aspects of observed phenomena may be determined by the kinetics of the process rather than by the relative thermodynamical stability of the two cluster types allowed within the system.

1. Introduction

In recent years, the Becker–Döring equations [3] have been generalized in a variety of ways and applied to many areas: from colloid chemistry [2, 5, 6], nucleation theory [14, 15] to RNA chain formation in the prebiotic world [16] and more general polymerisation reactions [1]. In this paper we generalize them with the aim of constructing a model of competitive nucleation, where two distinct types of cluster can be formed from the same basic monomer.

The problem of which morphology of crystal results from a crystallization experiment in which various types of crystal can be formed is a problem which has yet to be fully resolved. Experimentally, it is known that it is not necessarily the most thermodynamically stable form which nucleates first. Various explanations for this have been put forward, such as finite size effects [9], which can reverse the stability predicted by thermodynamic limits.

The approach adopted here is a generalization of an approach suggested by Kam *et al* [8]. We propose a thermodynamically consistent kinetic model which permits an equilibrium solution, and is sufficiently simple that properties of the solution at intermediate times can also be found. Whereas the Becker–Döring-style model proposed by Kam *et al* only allowed one type of cluster to form, we propose a model which allows two distinct types of cluster to form simultaneously. These could be two morphologies of crystal, or one of crystal and one amorphous or gel.

Initially we analyse the full problem in the aggregation-dominated limit. This builds on work in [18] where the standard Becker–Döring equations were analysed. The approach

0305-4470/99/498755+30$30.00

enables the sequence of timescales over which the process occurs to be identified, and approximate cluster distribution functions to be found for the times where one mechanism takes over from another as being the rate-determining step. However, much of the temporal evolution of the system remains unsolved, so an alternative approximation is used—namely the coarse-graining method. This method has been used in various applications [5, 7, 15], and has recently been analysed in more detail [7, 17, 18] in an attempt to assess its accuracy and validity. Using this method we uncover more of the kinetics of the process and are able to gain leading-order solutions for measurable macroscopic quantities.

In the remainder of this section we review the Becker–Döring system of equations and quote its basic properties. We give a brief summary of the coarse-grained reduction method which will be generalized later in the paper. Section 2 introduces a new model for competitive aggregation which is the principal subject of study in this paper. Due to the complexities of the new model—both in its nonlinearity and nonlocality—a general solution is not available. In section 3 an asymptotic solution is derived which demonstrates some of the phenomena describable by the new system of equations. Results from a numerical solution of the problem are also presented, confirming the validity of the asymptotic solution. An alternative approximate solution method is derived in section 4, where a coarse-graining procedure enables the passage from a microscopic model to a macroscopic one. This much simpler system is analysed in section 5 using dynamical systems theory, where asymptotic and numerical solutions are compared. The results are discussed in section 6.

1.1. Review of the Becker–Döring equations

Our model is based on the Becker–Döring system of equations for the growth of clusters. This system uses the concentrations of clusters of each aggregation number (r) as dependent variables, $c_r(t)$. The only mechanism by which clusters can grow or fragment is by the gain or loss of a single monomer at a time. Thus, if we represent a cluster of size r by C_r, we only allow reactions of the form

$$C_r + C_1 \rightleftharpoons C_{r+1}. \tag{1.1}$$

The forward reaction is assumed to occur at a rate a_r, and the reverse at rate b_{r+1}. We shall use the form of equations in which the total mass, or density, of material

$$\varrho = \sum_{r=1}^{\infty} r c_r \tag{1.2}$$

is constant. The kinetic equations for the concentrations are then

$$\dot{c}_r = J_{r-1} - J_r \qquad (r \geqslant 2) \tag{1.3}$$

$$J_r = a_r c_r c_1 - b_{r+1} c_{r+1} \tag{1.4}$$

$$\dot{c}_1 = -J_1 - \sum_{r=1}^{\infty} J_r. \tag{1.5}$$

As well as the conserved quantity (1.2), this system of equations has the physically relevant property of having a unique equilibrium solution, which we shall write as $c_r = Q_r c_1^r$, where Q_r is the partition function derived from the forward and backward rate coefficients by

$$a_r Q_r = b_{r+1} Q_{r+1} \qquad Q_1 = 1. \tag{1.6}$$

Also, there is a Lyapunov function

$$V = \sum_{r=1}^{\infty} c_r \left(\log\left(\frac{c_r}{Q_r} \right) - 1 \right) \tag{1.7}$$

provided this is bounded below. The existence of this function ensures that the equilibrium solution is approached regardless of the initial conditions specified. Finally, there is a weak form of the differential part of the system: for any sequence $\{g_r\}_{r=1}^{\infty}$, the identities

$$\sum_{r=1}^{\infty} g_r \dot{c}_r = \sum_{r=1}^{\infty} (g_{r+1} - g_r - g_1) J_r \tag{1.8}$$

hold. We shall require that these properties are maintained in any modification we make to the system of equations.

1.2. The coarse-graining process

The above system can be coarse-grained to obtain a set of equations which model the same process on a larger r-scale. This process is algorithmic in nature, and leads to a system of equations with a similar structure to the original system. Eliminating the concentration c_{r+1} from J_r and J_{r+1} leads to

$$a_{r+1} c_1 J_r + b_{r+1} J_{r+1} = a_r a_{r+1} c_{r+1} c_1^2 - b_{r+1} b_{r+2} c_{r+2} \tag{1.9}$$

and we define this quantity to be the flux from clusters of size r to size $r + 2$. This allows us to eliminate c_{r+1} from the system of equations. Such a procedure can be generalized so as to retain only one third, one quarter, or an arbitrary fraction of the dependent variables present in the original system.

We introduce a 'mesh function' Λ_n to represent the r-values of retained cluster sizes. Thus new concentration variables $\{x_n\}_{n=1}^{\infty}$ denote the concentrations $\{c_{\Lambda_n}\}_{n=1}^{\infty}$, and the concentrations of all other cluster sizes are eliminated from the system. In forming the coarse-grained model, we assume that all concentrations c_r with $\Lambda_{n-1} + 1 \leqslant r \leqslant \Lambda_n$ are equal to $c_{\Lambda_n} = x_n$. In general, the mesh spacing $\lambda_n = \Lambda_{n+1} - \Lambda_n$ can be allowed to vary with aggregation number, so that a non-uniform grid can be used to investigate some size ranges in more detail than others. However, for simplicity, here we shall use a uniform mesh in which $\Lambda_n = (n-1)\lambda + 1$. Note that, whatever mesh is chosen, one never eliminates the monomer concentration. This procedure leads to the system of equations

$$\begin{aligned} &\dot{x}_n = L_{n-1} - L_n \qquad (n \geqslant 2) \\ &L_n = \alpha_n x_n x_1^{\lambda} - \beta_{n+1} x_{n+1} \\ &\dot{x}_1 = -\lambda L_1 - \sum_{n=1}^{\infty} \lambda^2 L_n. \end{aligned} \tag{1.10}$$

Here, the new coefficients α_n, β_n are given by

$$\alpha_n = T a_{\Lambda_n} a_{\Lambda_n+1} \ldots a_{\Lambda_{n+1}-1} \qquad \beta_{n+1} = T b_{\Lambda_n+1} b_{\Lambda_n+2} \ldots b_{\Lambda_{n+1}}. \tag{1.11}$$

The constant T is included in both forward and backward rates since, as noted in [18], for maximum accuracy the contraction procedure should be accompanied by a change of timescale. Alternatively, including a change of timescale in the derivation of the new system of equations (1.10) from (1.3)–(1.5) allows the constant T to be scaled out.

The partition function (1.6) carries over to the modified system, with Q_{Λ_n} satisfying both $Q_{\Lambda_1} = 1$ and $\alpha_n Q_{\Lambda_n} = \beta_{n+1} Q_{\Lambda_{n+1}}$. This induces the equilibrium solution $x_n = Q_{\Lambda_n} x^{\Lambda_n}$, which agrees with the equilibrium solution of the original system $x_n = c_{\Lambda_n}$.

The new system (1.10) also has a conserved quantity which corresponds to density. Since the aggregation number of a particle represented by x_n is Λ_n, its mass is also proportional to Λ_n and there are λ of such cluster sizes in x_r, the density of the reduced system is then $\varrho = x_1 + \sum_{n=2}^{\infty} \lambda \Lambda_n x_n$. The function $V = x_1(\log x_1 - 1) + \sum_{n=2}^{\infty} \lambda x_n (\log(x_n / Q_{\Lambda_n}) - 1)$

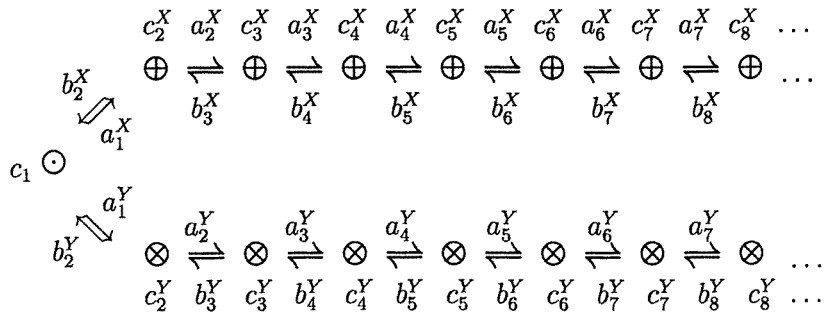

Figure 1. Diagrammatic summary of the model of competitive nucleation.

qualifies as a Lyapunov function under the same conditions as (1.7). Finally, for any sequence $\{h_n\}_{n=1}^{\infty}$

$$\sum_{n=1}^{\infty} h_n \dot{x}_n = (h_2 - \lambda h_1 - \lambda^2 h_1) L_1 + \sum_{n=2}^{\infty} (h_{n+1} - h_n - \lambda^2 h_1) L_n. \tag{1.12}$$

Thus, the reduced system shares the same physically relevant properties as the original system. Note, however, that the coarse-graining has accentuated the nonlinearity in the flux term of the new equations (1.10).

2. Proposed model

The model we propose allows two types or morphologies of clusters to form; the first, we shall denote by C_r^X and the other by C_r^Y, both form from the same monomer C_1. Thus the reactions we allow are of the form

$$C_r^X + C_1 \rightleftharpoons C_{r+1}^X \qquad C_r^Y + C_1 \rightleftharpoons C_{r+1}^Y. \tag{2.1}$$

Letting lower case variables denote concentrations, the kinetic equations are

$$\begin{aligned} \dot{c}_r^X &= J_{r-1}^X - J_r^X \qquad J_r^X = a_r^X c_r^X c_1 - b_{r+1}^X c_{r+1}^X \\ \dot{c}_r^Y &= J_{r-1}^Y - J_r^Y \qquad J_r^Y = a_r^Y c_r^Y c_1 - b_{r+1}^Y c_{r+1}^Y \\ \dot{c}_1 &= -J_1^X - J_1^Y - \sum_{r=1}^{\infty} J_r^X - \sum_{r=1}^{\infty} J_r^Y \end{aligned} \tag{2.2}$$

where c_r^X, c_r^Y represent the concentration of clusters of type X, Y respectively, and J_r^X, J_r^Y are the mass fluxes of material from aggregation number r to $r+1$ in each morphology. No cluster can change morphology from X to Y or vice versa; the only way mass can change from one form to the other is by the stepwise break-up of one cluster entirely into monomers (which have no morphology) and the subsequent reaggregation of monomers in the other form.

This system possesses the same four special properties as the original set of equations:

- A conserved quantity, which we refer to as the density of the system

$$\varrho = c_1 + \sum_{r=2}^{\infty} r(c_r^X + c_r^Y). \tag{2.3}$$

- A unique equilibrium solution

$$\bar{c}_r^X = Q_r^X \bar{c}_1^r \qquad \bar{c}_r^Y = Q_r^Y \bar{c}_1^r \tag{2.4}$$

where the Q_r^X, Q_r^Y functions are partition functions for the two types of cluster; they satisfy

$$Q_1^X = 1 \qquad Q_1^Y = 1 \qquad a_r^X Q_r^X = b_{r+1}^X Q_{r+1}^X \qquad a_r^Y Q_r^Y = b_{r+1}^Y Q_{r+1}^Y. \tag{2.5}$$

The partition functions can be related to the chemical potentials of the cluster morphologies; the chemical potential of clusters of size r and morphology X, Y is respectively μ_r^X, μ_r^Y where

$$\mu_r^X = \mu_r^{X\ominus} + kT \log c_r^X \qquad \mu_r^Y = \mu_r^{Y\ominus} + kT \log c_r^Y \tag{2.6}$$

respectively, and the chemical potential of monomers is $\mu_1 = \mu_1^{\ominus} + kT \log c_1$. At equilibrium, $c_r^X = Q_r^X c_1^r$, $c_r^Y = Q_r^Y c_1^r$, $\mu_r^X = r\mu_1 = \mu_r^Y$. Now, choosing a reference point in which $\mu_1^{\ominus} = 0$ implies

$$\mu_r^{X\ominus} = -kT \log Q_r^X \qquad \mu_r^{Y\ominus} = -kT \log Q_r^Y. \tag{2.7}$$

- A Lyapunov function

$$V = c_1(\log c_1 - 1) + \sum_{r=2}^{\infty} c_r^X \left(\log\left(\frac{c_r^X}{Q_r^X} \right) - 1 \right) + c_r^Y \left(\log\left(\frac{c_r^Y}{Q_r^Y} \right) - 1 \right). \tag{2.8}$$

  This decreases with time and corresponds to the free energy of the system.
- A set of identities; for a set of numbers $(g_1, \{g_r^X, g_r^Y\}_{r=2}^{\infty})$

$$g_1 \dot{c}_1 + \sum_{r=2}^{\infty} (g_r^X \dot{c}_r^X + g_r^Y \dot{c}_r^Y) = \sum_{r=1}^{\infty} (g_{r+1}^X - g_r^X - g_1) J_r^X + (g_{r+1}^Y - g_r^Y - g_1) J_r^Y. \tag{2.9}$$

To summarize, we have generalized the Becker–Döring equations to allow for different morphologies of cluster to grow from a single type of monomer. The new system is effectively two Becker–Döring systems coupled together through a more complicated equation for the monomer concentration. This combined system retains the useful structure of the original Becker–Döring model, having a unique equilibrium solution, conservation of density and having a well-defined Lyapunov function (free energy) which guarantees convergence to the equilibrium solution whatever initial conditions are imposed on the system.

The model allows the two morphologies to have different growth and fragmentation rates. These rates are typically size dependent, the aggregation rates having the form $a_r^X = a^X r^{1-1/d}$, $a_r^Y = a^Y r^{1-1/d}$ in cases where aggregation is surface-limited in d-dimensions. The fragmentation rates b_r^X, b_r^Y then depend on the relative stability of different cluster sizes; free-energy arguments can be used to deduce the shape of the partition functions, Q_r^X, Q_r^Y, and then (2.5) used to work back to b_r^X, b_r^Y. In many crystal growth scenarios it is known that there is a critical size, below which clusters are unstable and tend to fragment, and above which clusters tend to grow. These scenarios can be modelled by a chemical potential which is dependent only on bulk energy and surface energy, leading to a partition function of the form $kT \log Q_r = \nu(r-1) - \sigma(r-1)^{2/3}$, for example ($\nu$ being the coefficient of bulk energy and σ that of surface energy). However, such choices for the rate constants lead to equations which are only solvable numerically, a full general solution of the system (2.2) not being possible to find. So, here we consider a simpler example where both growth and fragmentation rates are size independent. In particular, we analyse the aggregation-dominated case with constant coefficients, where $a_r^X = 1$, $a_r^Y = a$, $b_r^X = \varepsilon$ and $b_r^Y = b\varepsilon$. In the case $\varepsilon \ll 1$, a solution is available through the use of matched asymptotic expansions: we expect the solution to pass through various timescales, initially fragmentation will not influence the system, but at later times this effect will become relevant.

There is interesting behaviour associated with this example. If $a > 1$ then we expect more clusters of type Y to form than of type X, whereas if $a < 1$ then the reverse will occur. However,

Table 1. The six ranges for a, b determining which morphology dominates the system initially and at equilibrium.

Parameters	Initial nucleation	Equilibrium configuration
$a > b > 1$	Y dominates initially	Y dominates at equilibrium
$a > 1 > b$	Y dominates initially	Y dominates at equilibrium
$b > a > 1$	Y dominates initially	X dominates at equilibrium
$b > 1 > a$	X dominates initially	X dominates at equilibrium
$1 > a > b$	X dominates initially	Y dominates at equilibrium
$1 > b > a$	X dominates initially	X dominates at equilibrium

the morphology which dominates at equilibrium depends on whether $a > b$ or $a < b$, type Y dominating in the former case and type X in the latter. At this level of description there are six combinations of parameters which can occur, as described in table 1. Lines three and five of this table are the most interesting, for in these cases one morphology of cluster is predominant at the start of the process but is more prone to fragmentation, so at later times the other type of cluster dominates. In these cases especially, the timescale and manner in which matter is transferred from one morphology to the other is of great interest.

3. Weak fragmentation case

In this section we aim to solve the problem outlined above, using matched asymptotic expansions to find the various stages through which the system proceeds as clusters are formed, as well as to determine the leading-order solutions.

With $a_r^X = 1$, $a_r^Y = a$, $b_r^X = \varepsilon$, $b_r^Y = b\varepsilon$, the problem can be formulated as

$$\begin{aligned}
&\dot{c}_r^X = c_{r-1}^X c_1 - \varepsilon c_r^X - c_r^X c_1 + \varepsilon c_{r+1}^X \qquad \dot{c}_r^Y = a c_{r-1}^Y c_1 - b\varepsilon c_r^Y - a c_r^Y c_1 + b\varepsilon c_{r+1}^Y \\
&\dot{c}_1 = \varepsilon c_2^X + b\varepsilon c_2^Y - c_1^2 - a c_1^2 + \varepsilon \sum_{r=1}^{\infty} c_{r+1}^X + \varepsilon b \sum_{r=1}^{\infty} c_{r+1}^Y - c_1 \sum_{r=1}^{\infty} c_r^X - a c_1 \sum_{r=1}^{\infty} c_r^Y .
\end{aligned} \tag{3.1}$$

For this system $Q_r^X = \varepsilon^{1-r}$, $Q_r^Y = (b\varepsilon/a)^{1-r}$. The initial conditions we are primarily concerned with are where all material starts in monomeric form, thus $c_1(0) = \varrho$, $c_r^X(0) = 0 = c_r^Y(0)$ for $r \geqslant 2$. However, our large-time asymptotic results will be more widely applicable, to any initial conditions with sufficiently rapid decay in the large-r limit.

Clearly the case $a = b$ is a special case since then the shape of the equilibrium solution for clusters of types X and Y will be the same. Other parameter values of interest will be $a = 1 \neq b$—where the initial stages of nucleation will be identical (aggregation dominated) but later will differ due to the different reverse reaction rates. If $b > a > 1$ then the aggregation of Y will initially be faster than that of X (due to $a > 1$) but later in the process we will expect more clusters of X since $c_1 \to \varepsilon$ and the cluster distribution function for Y will decay more rapidly than X (since $a < b$).

3.1. $t = \mathcal{O}(1)$

The first relevant timescale is where $t = \mathcal{O}(1)$, where the fragmentation terms have no effect at leading order. Over this timescale all concentrations are $\mathcal{O}(1)$, and evolve on the timescale $t = \mathcal{O}(1)$, so the effects of fragmentation are ignorable at leading order. Such a simplification means that exact explicit solutions are available—as was first noted for the standard Becker–Döring equations by Brilliantov and Kravitsky [4].

Thus, the system of equations we are concerned with is

$$\begin{aligned} \frac{\mathrm{d}c_r^X}{\mathrm{d}t} &= c_1(c_{r-1}^X - c_r^X) \qquad \frac{\mathrm{d}c_r^Y}{\mathrm{d}t} = c_1(c_{r-1}^Y - c_r^Y) \\ \frac{\mathrm{d}c_1}{\mathrm{d}t} &= -2(1+a)c_1^2 - c_1\sum_{r=2}^{\infty}(c_r^X + ac_r^Y) \end{aligned} \tag{3.2}$$

and we introduce a new timescale $\tau = \int_0^t c_1(s)\,\mathrm{d}s$ such that $\frac{\mathrm{d}}{\mathrm{d}\tau} = \frac{1}{c_1}\frac{\mathrm{d}}{\mathrm{d}t}$, in order to remove the nonlinearity from the problem. This yields the transformed equations

$$\begin{aligned} \frac{\mathrm{d}c_r^X}{\mathrm{d}\tau} &= c_{r-1}^X - c_r^X \qquad \frac{\mathrm{d}c_r^Y}{\mathrm{d}\tau} = c_{r-1}^Y - c_r^Y \\ \frac{\mathrm{d}c_1}{\mathrm{d}\tau} &= -2(1+a)c_1 - \sum_{r=2}^{\infty}(c_r^X + ac_r^Y). \end{aligned} \tag{3.3}$$

We introduce generating functions in order to solve for all the variables $\{c_r^X\}_{r=2}^{\infty}$ and $\{c_r^Y\}_{r=2}^{\infty}$ simultaneously. We define

$$F(x,\tau) = \sum_{r=2}^{\infty} x^r c_r^X(\tau) \qquad G(x,\tau) = \sum_{r=2}^{\infty} x^r c_r^Y(\tau). \tag{3.4}$$

The equations determining $F(x,\tau)$, $G(x,\tau)$ and $c_1(\tau)$ are then

$$\frac{\partial F}{\partial \tau} + (1-x)F = x^2 c_1(\tau) \tag{3.5}$$

$$\frac{\partial G}{\partial \tau} + a(1-x)G = ax^2 c_1(\tau) \tag{3.6}$$

$$\frac{\mathrm{d}c_1}{\mathrm{d}\tau} + 2(1+a)c_1 = -F_1(\tau) - aG_1(\tau). \tag{3.7}$$

Initially, we shall be concerned with the simpler system of three equations for $c_1(\tau)$, $F_1(\tau) = F(1,\tau)$ and $G_1(\tau) = G(1,\tau)$:

$$F_1'(\tau) = c_1(\tau) \qquad G_1'(\tau) = ac_1(\tau) \qquad c_1'(\tau) = -2(1+a)c_1(\tau) - F_1(\tau) - G_1(\tau) \tag{3.8}$$

which form a closed system.

Taking the ratio of the first two equations yields $G_1 = aF_1$ when it is noted that the initial conditions imply G_1 and F_1 are simultaneously zero. Now $c_1 = F_1'$ is used to construct a linear constant coefficient ordinary differential equation for F_1. Imposing the initial conditions $F_1(0) = 0$ and $c_1(0) = \varrho$ yields the solution

$$c_1 = \varrho \mathrm{e}^{-\tau(1+a)}\left[\cosh\left(\tau\sqrt{2a}\right) - \frac{(1+a)}{\sqrt{2a}}\sinh\left(\tau\sqrt{2a}\right)\right] \tag{3.9}$$

$$F_1 = \frac{\varrho \mathrm{e}^{-\tau(1+a)}}{\sqrt{2a}}\sinh\left(\tau\sqrt{2a}\right) \qquad G_1 = \frac{\varrho\sqrt{a}\mathrm{e}^{-\tau(1+a)}}{\sqrt{2}}\sinh\left(\tau\sqrt{2a}\right). \tag{3.10}$$

Now we are in a position to solve the x-dependent problem (3.5), (3.6). Now that $c_1(\tau)$ has been found, these equations can be integrated to give the generating functions

$$\begin{aligned} F(x,\tau) = \frac{\varrho x^2 \mathrm{e}^{-\tau}}{2\sqrt{2a}}\Bigg[&\left(\frac{1+a-\sqrt{2a}}{x+a-\sqrt{2a}}\right)(\mathrm{e}^{-\tau(a-\sqrt{2a})} - \mathrm{e}^{x\tau}) \\ &- \left(\frac{1+a+\sqrt{2a}}{x+a+\sqrt{2a}}\right)(\mathrm{e}^{-\tau(a+\sqrt{2a})} - \mathrm{e}^{x\tau})\Bigg] \end{aligned} \tag{3.11}$$

$$G(x,\tau) = \frac{\varrho\sqrt{a}x^2\mathrm{e}^{-a\tau}}{2\sqrt{2}}\left[\left(\frac{a+1-\sqrt{2a}}{ax+1-\sqrt{2a}}\right)(\mathrm{e}^{-\tau(1-\sqrt{2a})}-\mathrm{e}^{ax\tau}) - \left(\frac{a+1+\sqrt{2a}}{ax+1+\sqrt{2a}}\right)(\mathrm{e}^{-\tau(1+\sqrt{2a})}-\mathrm{e}^{ax\tau})\right]. \tag{3.12}$$

From these, it is now a simple matter to extract c_r^X and c_r^Y by expanding them as Taylor series in x. This yields

$$\begin{aligned} c_r^X &= \frac{\varrho\mathrm{e}^{-\tau}}{2\sqrt{2a}}\left[\left(\frac{1+a-\sqrt{2a}}{a-\sqrt{2a}}\right)\left(\frac{-1}{a-\sqrt{2a}}\right)^{r-2}\sum_{i=r-1}^{\infty}\frac{[-\tau(a-\sqrt{2a})]^i}{i!}\right. \\ &\quad \left. -\left(\frac{1+a+\sqrt{2a}}{a+\sqrt{2a}}\right)\left(\frac{-1}{a+\sqrt{2a}}\right)^{r-2}\sum_{i=r-1}^{\infty}\frac{[-\tau(a+\sqrt{2a})]^i}{i!}\right] \\ c_r^Y &= \frac{\varrho\sqrt{a}\mathrm{e}^{-a\tau}}{2\sqrt{2}}\left[\left(\frac{a+1-\sqrt{2a}}{1-\sqrt{2a}}\right)\left(\frac{-a}{1-\sqrt{2a}}\right)^{r-2}\sum_{i=r-1}^{\infty}\frac{[-\tau(1-\sqrt{2a})]^i}{i!}\right. \\ &\quad \left. -\left(\frac{a+1+\sqrt{2a}}{1+\sqrt{2a}}\right)\left(\frac{-a}{1+\sqrt{2a}}\right)^{r-2}\sum_{i=r-1}^{\infty}\frac{[-\tau(1+\sqrt{2a})]^i}{i!}\right]. \end{aligned} \tag{3.13}$$

This solution ceases to be valid when the monomer concentration drops to zero, this occurs at $\tau = \tau_c$ given by

$$\tau_c = \frac{1}{2\sqrt{2a}}\log\left(\frac{1+a+\sqrt{2a}}{1+a-\sqrt{2a}}\right). \tag{3.14}$$

As $\tau \to \tau_c$, $c_1 \to 0$, and when $c_1 = \mathcal{O}(\varepsilon)$, other terms enter the leading-order balance, and a new timescale is required. The second timescale is shifted by $K\log(1/\varepsilon)$ from the first. Since

$$t = \int_0^{\tau_c+\varepsilon\tau_2}\frac{\mathrm{d}\tau}{c_1(\tau)} \sim \int_{\kappa}^{\tau_c+\varepsilon\tau_2}\frac{K\,\mathrm{d}\tau}{(\tau_c-\tau)} \sim -K\log\varepsilon + \mathcal{O}(1) \tag{3.15}$$

(for some $\mathcal{O}(1)$ constant κ). The constant K is determined by $1/K = (-\frac{\mathrm{d}c_1}{\mathrm{d}\tau})|_{\tau=\tau_c}$, hence

$$K = \frac{\sqrt{1+a^2}}{\varrho(1+a)}\exp\left(\frac{(1+a)}{2\sqrt{2a}}\log\left(\frac{1+a+\sqrt{2a}}{1+a-\sqrt{2a}}\right)\right). \tag{3.16}$$

Unfortunately, due to the complexity of $c_1(\tau)$ in (3.9), it is not possible to explicitly relate the results (3.13), quoted in terms of τ, back to the original timescale t.

3.2. $t = K\log(1/\varepsilon) + \mathcal{O}(1)$

This timescale is defined by $t = K\log(1/\varepsilon) + t_2$ where $t_2 = \mathcal{O}(1)$ and over this timescale $c_1 = \varepsilon C_1$, with all other concentrations $\{c_r^X\}_{r=2}^{\infty}$ and $\{c_r^Y\}_{r=2}^{\infty}$ remaining $\mathcal{O}(1)$. To leading order:

$$\frac{\mathrm{d}c_r^X}{\mathrm{d}t_2} = 0 \qquad \frac{\mathrm{d}c_r^Y}{\mathrm{d}t_2} = 0 \qquad \frac{\mathrm{d}C_1}{\mathrm{d}t_2} = c_2^X + bc_2^Y + \sum_{r=1}^{\infty}(c_{r+1}^X + bc_{r+1}^Y) - C_1\sum_{r=2}^{\infty}(c_r^X + ac_r^Y). \tag{3.17}$$

Thus, all concentrations except that of the monomers remain constant, which implies the equation governing C_1 is linear, so over this timescale the monomer concentration relaxes to its pseudo-equilibrium value

$$C_1 \to C_1^{\dagger} \stackrel{\text{def}}{=} \frac{\sum_{r=2}^{\infty}(c_r^X + bc_r^Y)}{\sum_{r=2}^{\infty}(c_r^X + ac_r^Y)} + \frac{c_2^X + bc_2^Y}{\sum_{r=2}^{\infty}(c_r^X + ac_r^Y)} \qquad \text{as} \quad t_2 \to \infty. \tag{3.18}$$

As $t_2 \to \infty$ all concentrations are constant, and so the next timescale will be considerably longer.

3.3. $t = \mathcal{O}(\varepsilon^{-1})$

Since the rescaled monomer concentration $C_1 = c_1/\varepsilon$ tends to an $\mathcal{O}(1)$ constant at the end of the previous timescale while all the other concentrations remain order one constants, we must maintain these scalings, in the new timescale, and analyse the system over a longer timescale, which is defined by $t_3 = \varepsilon t$. Thus, our governing equations are

$$\frac{\mathrm{d}c_r^X}{\mathrm{d}t_3} = C_1 c_{r-1}^X - C_1 c_r^X - c_r^X + c_{r+1}^X \tag{3.19}$$

$$\frac{\mathrm{d}c_r^Y}{\mathrm{d}t_3} = aC_1 c_{r-1}^Y - aC_1 c_r^Y - bc_r^Y + bc_{r+1}^Y \tag{3.20}$$

$$\varepsilon\frac{\mathrm{d}C_1}{\mathrm{d}t_3} = c_2^X + bc_2^Y - a\varepsilon C_1^2 - \varepsilon C_1^2 + b\sum_{r=1}^{\infty} c_{r+1}^Y + \sum_{r=1}^{\infty} c_{r+1}^X - aC_1\sum_{r=1}^{\infty} c_r^Y - C_1\sum_{r=1}^{\infty} c_r^X. \tag{3.21}$$

At leading order, equation (3.21) implies that the monomer concentration remains in equilibrium with the rest of the system at all times, thus $C_1 = C_1^\dagger$ as given by (3.18). The other equations, however, are not explicitly soluble.

To gain an intuitive understanding of the behaviour of the system over this timescale, we investigate the temporal evolution of some macroscopic quantities associated with the cluster distribution functions. We define new quantities $N_X(t_3)$, $N_Y(t_3)$ to denote the total number of clusters of each type, and $\varrho_X(t_3)$, $\varrho_Y(t_3)$ representing the total density (mass) in each morphology. These are defined by

$$N_X = \sum_{r=2}^{\infty} c_r^X \qquad N_Y = \sum_{r=2}^{\infty} c_r^Y \qquad \varrho_X = \sum_{r=2}^{\infty} rc_r^X \qquad \varrho_Y = \sum_{r=2}^{\infty} rc_r^Y. \tag{3.22}$$

All these are time-dependent quantities, with the densities satisfying $\varrho_X + \varrho_Y + c_1 = \varrho$ independent of time, although $c_1 = \mathcal{O}(\varepsilon)$ implies that $\varrho = \varrho_X + \varrho_Y$ at leading order. Using (3.18) and (3.19), (3.20), the new quantities we have introduced satisfy the differential equations

$$\frac{\mathrm{d}}{\mathrm{d}t_3}N_X = -c_2^X \qquad \frac{\mathrm{d}}{\mathrm{d}t_3}N_Y = -bc_2^Y \tag{3.23}$$

$$\frac{\mathrm{d}\varrho_X}{\mathrm{d}t_3} = (C_1 - 1)N_X - c_2^X \qquad \frac{\mathrm{d}\varrho_Y}{\mathrm{d}t_3} = (aC_1 - b)N_Y - bc_2^Y. \tag{3.24}$$

Using the fact that C_1 is given by $(N_X + bN_Y + c_2^X + bc_2^Y)/(N_X + aN_Y)$, (see (3.18)), the above can be rewritten as

$$\frac{\mathrm{d}\varrho_X}{\mathrm{d}t_3} = \frac{(b-a)N_X N_Y}{N_X + aN_Y} + \frac{bc_2^Y N_X - ac_2^X N_Y}{N_X + aN_Y} \tag{3.25}$$

$$\frac{\mathrm{d}\varrho_Y}{\mathrm{d}t_3} = \frac{(a-b)N_X N_Y}{N_X + aN_Y} + \frac{ac_2^X N_Y - bc_2^Y N_X}{N_X + aN_Y}. \tag{3.26}$$

In this form, it is clear that (3.25), (3.26) satisfy $\frac{\mathrm{d}}{\mathrm{d}t_3}(\varrho_X + \varrho_Y) = 0$ implying conservation of density at leading order, as noted above.

Clearly (3.23), (3.24) do not form a closed system of equations, but they do help us understand the dynamics occurring on this timescale. Since all terms from the original equations now enter the leading-order balance, towards the end of this timescale we expect a local equilibrium to become established in which clusters of small size equilibrate with the monomer concentration. Thus, we expect c_2^X and c_2^Y to become small. Formally, equilibrium is given by $c_2^X = \varepsilon C_1^2$, and $c_2^Y = a\varepsilon C_1^2/b$, but since c_2^X, c_2^Y are $\mathcal{O}(1)$ over this timescale,

at leading order we expect $c_2^X, c_2^Y \to 0$ as $t_3 \to \infty$. The dominant part of (3.18) is then $C_1 \sim (N_X + bN_y)/(N_X + aN_y)$.

The main feature of (3.25), (3.26) is the transfer of mass from one type of cluster to the other. If $a > b$ then mass is passed from X to Y and if $a < b$ then the transfer is in the opposite direction. The process by which this happens is the stepwise breakdown of clusters into monomers, which then aggregate with existing clusters of the other morphology: (3.23) implies no new clusters are formed. This transfer of matter occurs with the monomer concentration remaining very small: the kinetics thus proceed very slowly. Since the monomer concentration is $\mathcal{O}(\varepsilon)$, and an $\mathcal{O}(1)$ amount of mass has to be converted, the process takes an $\mathcal{O}(\varepsilon^{-1})$ length of time—hence the current timescale. To find asymptotic approximations to the shape of the cluster distribution function requires us to consider several cases separately as follows.

3.3.1. Special case: $a = b$. In this case, as $t_3 \to \infty$ differences in concentration between clusters of similar size and the same morphology will be smoothed out. Thus the long-time asymptotics of (3.19), (3.20) can be found by taking the continuum limit of the equations. We denote solutions of the continuum equations by $c^X(r, t)$, $c^Y(r, t)$. Equations (3.19), (3.20) are replaced by

$$\frac{\partial c^X}{\partial t_3} = \frac{1}{2}(1 + C_1^\dagger)\frac{\partial^2 c^X}{\partial r^2} + (1 - C_1^\dagger)\frac{\partial c^X}{\partial r} \tag{3.27}$$

$$\frac{\partial c^Y}{\partial t_3} = \frac{1}{2}a(1 + C_1^\dagger)\frac{\partial^2 c^Y}{\partial r^2} + a(1 - C_1^\dagger)\frac{\partial c^Y}{\partial r}. \tag{3.28}$$

In this case $C_1 \to 1$ as $t_3 \to \infty$; later, we verify that $c_2^X + ac_2^Y \ll N_X + N_Y$, and hence show that (3.18) implies $C_1 \to 1$. The equations for c^X, c^Y thus reduce to

$$\frac{\partial c^X}{\partial t_3} = \frac{\partial^2 c^X}{\partial r^2} \qquad \frac{\partial c^Y}{\partial t_3} = a\frac{\partial^2 c^Y}{\partial r^2} \tag{3.29}$$

which have the similarity solutions

$$c^X = \frac{K_X r \mathrm{e}^{-r^2/4t_3}}{t_3^{3/2}} \qquad c^Y = \frac{K_Y r \mathrm{e}^{-r^2/4at_3}}{t_3^{3/2}} \tag{3.30}$$

for constants K_X, K_Y. This solution can now be used to check that $c_2^X + ac_2^Y \ll N_X + aN_Y$, since c_2^X, c_2^Y are both $\mathcal{O}(t_3^{-3/2})$ as $t_3 \to \infty$ whereas $N_X, N_Y = \mathcal{O}(t_3^{-1/2})$, hence $C_1 \to 1$ as mentioned above. One constraint on the constants K_X, K_Y is conservation of density, which yields the equation $K_X + a^{3/2}K_Y = \varrho/2\sqrt{\pi}$. The solution for c^Y is obtained from the solution for c^X by replacing t with at. This implies $K_Y = K_X/a^{3/2}$, hence $K_X = \varrho/4\sqrt{\pi}$ and $K_Y = \varrho/4a^{3/2}\sqrt{\pi}$.

3.3.2. General case: $a < b$. Over this timescale the introduction of fragmentation into the leading-order balance means that the stability of X over Y takes effect. Virtually all the mass is transformed into the X-form, through the fragmentation of Y-clusters providing monomers which are then added to the population of growing X-clusters. The quantity C_1 remains $\mathcal{O}(1)$, being determined by (3.18), but decays due to the decay of c_2^X, c_2^Y and changes in N_X, N_Y.

At larger times, we expect the concentration of clusters with small aggregation numbers to tend to their equilibrium configuration subject to the present monomer concentration. In particular, $c_2^X \to \varepsilon C_1^2$ and $c_2^Y \to \varepsilon a C_1^2/b$, but since we are concerned with $c_2^X, c_2^Y = \mathcal{O}(1)$

in this timescale, we expect $c_2^X, c_2^Y \to 0$ as $t_3 \to \infty$. Thus, at larger times, the macroscopic densities ϱ_X, ϱ_Y are governed by

$$\frac{\mathrm{d}\varrho_X}{\mathrm{d}t_3} \approx N_X(C_1 - 1) \qquad \frac{\mathrm{d}\varrho_Y}{\mathrm{d}t_3} \approx N_Y(aC_1 - b). \tag{3.31}$$

Since $\varrho_X(t_3) + \varrho_Y(t_3) = \varrho$, $\mathrm{d}\varrho_X/\mathrm{d}t_3$ and $\mathrm{d}\varrho_Y/\mathrm{d}t_3$ must have opposite signs. Thus, C_1 must lie between unity and $b/a > 1$. The increase of the mass ϱ_X will be halted in the limit $t_3 \to \infty$ by $C_1 \to 1$; and to stop the consequent decrease in ϱ_Y, we must have $N_Y \to 0$.

In more detail, in the large-time limit the problem for c^Y reduces to the constant monomer Becker–Döring problem

$$\frac{\mathrm{d}c_r^Y}{\mathrm{d}t_3} = ac_{r-1}^Y - bc_r^Y - ac_r^Y + bc_{r+1}^Y \qquad (r \geqslant 3) \tag{3.32}$$

$$\frac{\mathrm{d}c_2^Y}{\mathrm{d}t_3} = -bc_2^Y - ac_2^Y + bc_3^Y \tag{3.33}$$

the form of whose solution is known [18]: formally, this approaches the equilibrium configuration $c_r^Y = c_1(a/b)^{r-1}$, over timescales of $t_3 = \mathcal{O}(1)$. This is formal since $c_1 = \mathcal{O}(\varepsilon)$, so the equilibrium solution satisfies $c_r = \mathcal{O}(\varepsilon)$ for all r, whereas in the current timescale we have adopted the scaling $c_r^Y = \mathcal{O}(1)$. So, to leading order, all we observe is $c_r^Y \to 0$ as $t_3 \to \infty$, with new scalings becoming necessary when c_r^Y reaches $\mathcal{O}(\varepsilon)$. When the concentrations $c_r^Y = \mathcal{O}(\varepsilon)$, their evolution is still on the timescale $t_3 = \varepsilon t = \mathcal{O}(1)$. Putting $c_r^Y = \varepsilon C_r^Y$ with $C_r^Y = \mathcal{O}(1)$, we find the problem for C_r^Y is

$$\frac{\mathrm{d}C_r^Y}{\mathrm{d}t_3} = aC_{r-1}^Y - bC_r^Y - aC_r^Y + bC_{r+1}^Y \qquad (r \geqslant 2) \tag{3.34}$$

with $C_1 = 1$, which is subtly different to (3.32), (3.33). This system approaches the equilibrium configuration

$$C_r^Y = C_1\left(\frac{a}{b}\right)^{r-1} \tag{3.35}$$

on the $t_3 = \varepsilon t = \mathcal{O}(1)$ timescale.

The solution for c^X over this timescale, as for c^Y, is only available in the limit $t_3 \to \infty$. Here, (3.19) can be replaced by the continuum limit

$$\frac{\partial c^X}{\partial t_3} = \frac{1}{2}(1 + C_1)\frac{\partial^2 c^X}{\partial r^2} + (1 - C_1)\frac{\partial c^X}{\partial r} \tag{3.36}$$

since the long timescale allows differences in concentration to be smoothed out. Our assumption that $C_1 \to 1$ as $t_3 \to \infty$ implies the advection term disappears and the resulting purely diffusive problem has the similarity solution

$$c^X = \frac{K_X r \mathrm{e}^{-r^2/4t_3}}{t_3^{3/2}}. \tag{3.37}$$

For large times, this agrees with the assumption of $c_r^X \to 0$ as $t_3 \to \infty$ at small r. Consideration of the macroscopic quantities (3.22) implies the constant K_X is $\varrho/4\sqrt{\pi}$. The long-time behaviour of the distribution of X-clusters is characterized by a single maximum in aggregation space (r) which moves to larger r-values and spreads out as time progresses.

Finally, for consistency, we need to verify the underlying assumption that $C_1 \to 1$ as $t_3 \to \infty$. From (3.37), as $t_3 \to \infty$, $N_X \sim t_3^{-1/2}$ and $c_2^X \sim t^{-3/2}$. Now c_2^Y asymptotes to an $\mathcal{O}(\varepsilon)$ constant; and in the large-time limit, the distribution c_r^Y becomes $\mathcal{O}(\varepsilon)$, and decays rapidly enough in r for N_Y to be $\mathcal{O}(\varepsilon)$ also. Thus the dominant term in (3.18) as $t_3 \to \infty$ is N_X, implying $C_1 \to 1$ as originally assumed.

Over this timescale, the greater thermodynamic stability of X over Y has taken effect, with the consequence that there is little mass left in the Y-form. However, the population of X-clusters has not yet reached equilibrium, so kinetics now proceed over an even longer timescale.

3.3.3. General case: $a > b$. The analysis for this case follows the above general case very closely, with X and Y swapping roles and the thermodynamic stability of Y being manifest through the loss of nearly all of the X-clusters. We formulate the problem for the timescale t_3, but the resulting equations can only be solved in the large-t_3 limit. The monomer concentration, given by (3.18), decreases, as c_2^X, c_2^Y become $\mathcal{O}(\varepsilon)$. At larger times, $b/a < C_1 < 1$, and (3.31) implies the growth of ϱ_Y at the expense of ϱ_X. In the limit $t_3 \to \infty$, we thus expect $C_1 \to b/a < 1$ with $N_X \to 0$. These assumptions will be verified later.

The concentrations c_r^X all tend to zero as $t_3 \to \infty$. Their subsequent evolution to equilibrium also occurs on the $t_3 = \varepsilon t = \mathcal{O}(1)$ timescale with the scalings $c_r^X = \varepsilon C_r^X$ and $C_r^X = \mathcal{O}(1)$ leading to

$$\frac{\mathrm{d}C_r^X}{\mathrm{d}t_3} = \frac{b}{a}C_{r-1}^X - C_r^X - \frac{b}{a}C_r^X + C_{r+1}^X. \tag{3.38}$$

Thus as $t_3 \to \infty$, $c_r^X \to \varepsilon(b/a)^r$. Over large times, the Y-distribution becomes slowly varying in aggregation number (r), so the continuum limit

$$\frac{\partial c^Y}{\partial t_3} = \frac{1}{2}(b + aC_1)\frac{\partial^2 c^Y}{\partial r^2} + (b - aC_1)\frac{\partial c^Y}{\partial r} \tag{3.39}$$

can be taken. Since $C_1 \to b/a$, the advection term disappears enabling (3.39) to be solved by the similarity solution

$$c^Y = \frac{\varrho r \mathrm{e}^{-r^2/4bt_3}}{4\sqrt{\pi}(bt_3)^{3/2}}. \tag{3.40}$$

Thus in the large-time limit, the majority of mass is contained within c^Y in a single-peaked distribution, the position of which moves to increasingly large aggregation numbers; there is negligible mass in the X-morphology.

All that remains for us to do now is to verify the initial assumptions; namely to show that in the large-time limit, (3.18) implies C_1 asymptotes to b/a. From (3.40), we have $N_Y \sim t_3^{-1/2}$ and $c_2^Y \sim t_3^{-3/2}$ in the large-time limit. We also have c_2^X becoming $\mathcal{O}(\varepsilon)$ over this timescale, as does N_X, since all the c_r^X approach equilibrium. Thus in the large-time limit, N_Y dominates (3.18), and $C_1 \to b/a$.

3.4. $t = \mathcal{O}(\varepsilon^{-2})$

At the end of the previous timescale, which ever subcase our system falls into, all the concentrations became small, so the scalings in this timescale must take account of this. We introduce the new scalings

$$c_r^X = \varepsilon C^X \qquad c_r^Y = \varepsilon C^Y \qquad t = \varepsilon^{-2} t_4 \tag{3.41}$$

to complement the existing $c_1 = \varepsilon C_1$.

3.4.1. Special case: $a = b$. We have already seen that the scaled monomer concentration $C_1 = c_1/\varepsilon$ approaches unity at the end of the previous timescale. In order to develop the longer-time kinetics we need the next-order correction term

$$C_1 = 1 + \varepsilon^{1/2} D_1 \tag{3.42}$$

so that $c_1 \sim \varepsilon + \varepsilon^{3/2} D_1(t_4)$.

Over the previous timescale, there was an $\mathcal{O}(1)$ mass in both X- and Y-forms: the matter in the system was spread over a wide range of aggregation numbers, each cluster size having a small concentration. Our primary concern in this timescale is with asymptotically large aggregation numbers, and in order to balance terms in the determining equations, we take $r = \varepsilon^{-1/2} z$ with $z = \mathcal{O}(1)$. Since the concentrations vary slowly with aggregation number, it is valid to take the continuum limit

$$\begin{aligned} \frac{\partial C^X}{\partial t_4} &= \frac{\partial^2 C^X}{\partial z^2} - D_1(t_4) \frac{\partial C^X}{\partial z} \\ \frac{1}{a} \frac{\partial C^Y}{\partial t_4} &= \frac{\partial^2 C^Y}{\partial z^2} - D_1(t_4) \frac{\partial C^Y}{\partial z}. \end{aligned} \tag{3.43}$$

There is a simpler 'inner' region, for $r = \mathcal{O}(1)$ characterized at leading order by the equations

$$0 = C^X_{r-1} - 2C^X_r + C^X_{r+1} \qquad 0 = C^Y_{r-1} - 2C^Y_r + C^Y_{r+1} \tag{3.44}$$

with solutions $C^X_r = 1 + (r-1)\tilde{K}_{4X}$, $C^Y_r = 1 + (r-1)\tilde{K}_{4Y}$. At large-$r$, this must match with the small-z solution of (3.43). In order to close the system of equations, we need to specify D_1. This is obtained by requiring density to be conserved. At leading order the density is given by $\varrho = \int_0^\infty z(C^X + C^Y)\mathrm{d}z$. Taking the time-derivative of this, and using (3.43), leads to

$$D_1(t_4) = -(1+a) \Big/ \int_0^\infty C^X(z, t_4) + aC^Y(z, t_4)\mathrm{d}z. \tag{3.45}$$

The system (3.43) together with (3.45) cannot be solved for arbitrary t_4, but the large-time kinetics can be found. As $t_4 \to \infty$, the system converges to a time-independent state; in order to satisfy the boundary conditions $C^X, C^Y \to 0$ as $z \to \infty$, this solution must have the form

$$C^X \to K_{4X} \exp(\overline{D}_1 z) \qquad C^Y \to K_{4Y} \exp(\overline{D}_1 z) \qquad D_1 \to \overline{D}_1 < 0 \quad \text{as} \quad t_4 \to \infty. \tag{3.46}$$

This solution has three parameters still to be specified, K_{4X}, K_{4Y}, $\overline{D}_1$. The first two are found by matching the above solution to the 'outer' problem to the solution of the 'inner' discrete problem. In order to match the solution of the inner problem (3.44) with the outer solution, $K_{4X} = 1 = K_{4Y}$ and $\tilde{K}_{4X} = 0 = \tilde{K}_{4Y}$. Finally, we are in a position to determine the value of the final parameter from (3.46), $\overline{D}_1$. Density conservation implies $\overline{D}_1$ must satisfy $\varrho = 2\int_0^\infty z \exp(\overline{D}_1 z)\mathrm{d}z$, giving $\overline{D}_1 = -\sqrt{2/\varrho}$ and hence the large-time asymptotic solution is

$$c_1 = \varepsilon - \varepsilon^{3/2}\sqrt{2/\varrho} \qquad c^X_r = c^Y_r = \varepsilon \exp\left(-r\sqrt{2\varepsilon/\varrho}\right). \tag{3.47}$$

3.4.2. General case: $a < b$. At the end of the previous timescale, the number of Y-clusters decayed, with the distribution of X-clusters being given by the similarity solution (3.37), subject to $c_1 = \varepsilon C_1 = \varepsilon$. Here, in order to determine the X-cluster distribution function we shall again need the first correction term to the monomer concentration, which has the form $C_1 = 1 + \varepsilon^{1/2} D_1$. Since the leading-order term in C_1 does not alter over this timescale, the solution (3.35) for the Y-clusters remains valid throughout this timescale. Thus we only consider the X-clusters in this section, the Y-clusters already being at equilibrium.

For X-clusters with $\mathcal{O}(1)$ aggregation numbers, the scalings (3.41) imply the governing equations

$$0 = C^X_{r-1} - 2C^X_r + C^X_{r+1} \tag{3.48}$$

with solution $C^X_r = 1 + (r-1)\tilde{K}_{4X}$, where $\tilde{K}_{4X}$ is an arbitrary constant to be determined by matching to the solution of the outer problem. Clearly this solution cannot be valid for all r.

If $\tilde{K}_{4X} < 0$ then the concentration would become negative at some large r, and if $\tilde{K}_{4X} \geqslant 0$ then the density would be divergent. Thus there must be a large-r region where other terms enter the leading-order balance of terms in the governing equations. This can also be deduced from the form of the similarity solution (3.37).

We continue to use the continuum limit, following its use at the end of the previous timescale, but now need to find the cluster size where kinetics are occurring. Balancing terms in the continuum equations yields $r = \varepsilon^{-1/2} z$ with $z = \mathcal{O}(1)$ and

$$\frac{\partial C^X}{\partial t_4} = \frac{\partial^2 C^X}{\partial z^2} - D_1(t_4) \frac{\partial C^X}{\partial z}. \tag{3.49}$$

The quantity $D_1(t_4)$ is obtained by requiring the density to be conserved. The leading-order contribution to the density comes from the outer region, whence the above scalings imply $\varrho = \int_0^\infty z C^X(z, t_4)\, \mathrm{d}z$. Taking the time derivative of this, and using (3.49), leads to

$$D_1(t_4) = -1 \Big/ \int_0^\infty C^X(z, t_4) \mathrm{d}z. \tag{3.50}$$

Unfortunately, systems such as this cannot be solved explicitly, but their large-time behaviour can be found. Assuming $D_1 \to \overline{D}_1$ as $t_4 \to \infty$, we find $C^X = K_{4X} \exp(\overline{D}_1 z)$, and matching this solution in the limit $z \to 0$ to the solution of (3.48) in the limit $r \to \infty$ yields $\tilde{K}_{4X} = 0$ and $K_{4X} = 1$. Conservation of density then gives $\overline{D}_1 = -1/\sqrt{\varrho}$. Thus the solution, over this timescale, tends to

$$c_1 = \varepsilon - \frac{\varepsilon^{3/2}}{\sqrt{\varrho}} \qquad c_r^X = \varepsilon \exp\left(-r\sqrt{\frac{\varepsilon}{\varrho}}\right) \tag{3.51}$$

together with $c_r^Y = \varepsilon C_r^Y$, where C_r^Y is given by equation (3.35).

3.4.3. General case: $a > b$. The leading-order kinetics which occur over this timescale is the redistribution of mass within the Y-distribution from the similarity solution (3.40) to equilibrium. The monomer concentration remains constant at leading order, which implies that the distribution of X-cluster remains constant also, and continues to be given by $c_r^X = \varepsilon(b/a)^r$ since it was already in equilibrium with the monomer concentration at the end of the previous timescale. In order to determine the evolution of the Y-cluster distribution, we need a higher-order term in the monomer concentration, thus

$$C_1 = \frac{b}{a}[1 + \varepsilon^{1/2} D_1(t_4)]. \tag{3.52}$$

For small cluster sizes (r), the leading-order determining equations for C_r^Y are

$$0 = bC_{r-1}^Y - bC_r^Y - bC_r^Y + bC_{r+1}^Y \tag{3.53}$$

together with $C_1 = b/a$, which are solved by $C_r^Y = b/a + \tilde{K}_{4Y}(r-1)$. At larger r, however, higher-order terms become relevant. Seeking a large-r region where other terms enter the leading-order balance leads to $r = \varepsilon^{-1/2} z$ with $z = \mathcal{O}(1)$, then

$$\frac{\partial C^Y}{\partial t_4} = b\frac{\partial^2 C^Y}{\partial z^2} - bD_1(t_4)\frac{\partial C^Y}{\partial z}. \tag{3.54}$$

Here D_1 is determined by conservation of density ($\varrho \sim \int_0^\infty z C^Y(z, t_4)\, \mathrm{d}z$), giving

$$D_1(t_4) = -b/a \int_0^\infty C^Y(z, t_4) \mathrm{d}z. \tag{3.55}$$

Unfortunately, a full solution cannot be determined, so we are once again forced to consider only the large-time asymptotics of this timescale. At large times (3.54) implies $C^Y \to$

$(b/a)\exp(\overline{D}_1 z)$, with $D_1 \to \overline{D}_1 < 0$ as $t_4 \to \infty$. Equating the density of this solution to ϱ then implies $\overline{D}_1 = -\sqrt{b/a\varrho}$. This outer solution matches correctly into the solution of the inner problem with $\tilde{K}_{4Y} = 0$. This is the equilibrium solution of the entire system and agrees with the equilibrium solution derived from the discrete equations, as will be shown in the next section.

3.5. Equilibrium

Sections 1 and 2 discussed the form of the equilibrium solution for arbitrary choices of the coefficients a_r, b_r. Here, since we have fixed forms for these coefficients, we can be more explicit about the equilibrium solution. We continue to use partition functions, now defining them explicitly, by

$$Q_r^X = \varepsilon^{1-r} \qquad Q_r^Y = \left(\frac{b\varepsilon}{a}\right)^{1-r}. \tag{3.56}$$

The monomer concentration c_1 at equilibrium depends on the total density in the system. Expanding the monomer concentration as $c_1 = \varepsilon C_1(1 + \varepsilon^p D_1)$, we find an equation relating the density to c_1 from (2.3):

$$\varrho = \varepsilon C_1(1+\varepsilon^p D_1)\left[\frac{1}{(1-C_1-\varepsilon^p C_1 D_1)^2} + \frac{1}{(1-\frac{a}{b}C_1 - \frac{a}{b}C_1\varepsilon^p D_1)^2}\right]. \tag{3.57}$$

An expansion of this expression in powers of ε yields $\varrho = \mathcal{O}(\varepsilon)$ unless $C_1 = 1$ or $C_1 = b/a$. Thus for $\mathcal{O}(1)$ values of ϱ, we expect C_1 to take on one of these values.

3.5.1. Special case $a = b$. In the special case $a = b$, the leading-order monomer concentration (c_1) can only tend to ε (that is $C_1 = 1$). Since the density is then $\mathcal{O}(\varepsilon^{1-2p})$, for $\varrho = \mathcal{O}(1)$ we must have $p = \frac{1}{2}$: the correction term is then $\mathcal{O}(\varepsilon^{3/2})$. Thus we put

$$c_1 \sim \varepsilon(1 + D_1\sqrt{\varepsilon}) \tag{3.58}$$

which, with $Q_r^X = Q_r^Y = \varepsilon^{1-r}$ gives the equilibrium solutions as $c_r^X = c_r^Y = \varepsilon(1 + D_1\sqrt{\varepsilon})^r$. Equating the density in this equilibrium solution to ϱ yields $D_1 = -\sqrt{2/\varrho}$ as the leading-order solution of

$$\varrho = \frac{2(1 + D_1\sqrt{\varepsilon})(1 + D_1^2\varepsilon)}{D_1^2} + \varepsilon + D_1\varepsilon^{3/2}. \tag{3.59}$$

The solution is thus $c_r^X = c_r^Y = \varepsilon(1 - \sqrt{2\varepsilon/\varrho})^r$, which agrees with (3.47) in the large-r limit. All a-dependence has disappeared from this expression, as is to be expected for the equilibrium solution, since a corresponds to the timescale over which the concentrations of Y-clusters evolve.

3.5.2. General case $a < b$. If $a \neq b$ then there are two similar subcases to consider: (i) $a > b$; (ii) $a < b$. In this latter case, $C_1 = 1$, since if $C_1 = b/a$ then the concentration of X-clusters is unbounded at large r.

Defining $c_1 = \varepsilon + D_1\varepsilon^{3/2}$ with $Q_r^X = \varepsilon^{1-r}$ and $Q_r^Y = (a\varepsilon/b)^{1-r}$ leads to

$$c_r^X = \varepsilon(1 + D_1\sqrt{\varepsilon})^r \qquad c_r^Y = \varepsilon\left(\frac{a}{b}\right)^{r-1}(1 + D_1\sqrt{\varepsilon})^r. \tag{3.60}$$

Thus all concentrations are small, but those of type Y decay much faster with increasing aggregation number (r) than those of the X-type. The net effect is that the mass in Y-form is only $a\varepsilon(2b-a)/(b-a)^2$, whereas the mass in the X-form is $\mathcal{O}(1)$, so that to leading-order in ε all mass is of the X-type and $D_1 = -1/\sqrt{\varrho}$.

3.5.3. General case $a > b$. The case $a > b$ is handled in a similar manner, with the roles of X and Y reversed. Now $c_1 = b\varepsilon/a + \mathcal{O}(\varepsilon^{3/2})$, since if $c_1 = \varepsilon + \mathcal{O}(\varepsilon^{3/2})$ then the Y-distribution would diverge in the large-r limit. The equilibrium solution is

$$c_r^X = \varepsilon \left(\frac{b}{a}\right)^r \left(1 - \sqrt{\frac{b\varepsilon}{a\varrho}}\right)^r \qquad c_r^X = \varepsilon \left(\frac{b}{a}\right) \left(1 - \sqrt{\frac{b\varepsilon}{a\varrho}}\right)^r \qquad c_1 = \frac{b\varepsilon}{a}\left(1 - \sqrt{\frac{b\varepsilon}{a\varrho}}\right) \tag{3.61}$$

the majority of the mass ending up in the Y-form.

Thus in all cases, the scalings are the same in magnitude, namely $c_r = \mathcal{O}(\varepsilon)$, but the special case $a = b$ (3.58) is not simply a subcase of the general results (3.60) or (3.61).

3.6. Summary of results from asymptotic analysis

The asymptotic solution passes through four timescales. In the first, clusters of both types grow at the expense of the monomer: this timescale ends when the monomer concentration becomes small and thus slows the growth of clusters. There are no effects of fragmentation in this timescale; many clusters form, the vast majority having relatively small aggregation numbers—typically up to ten. In the second timescale, which is shifted to larger times, but as fast as the first, the monomer concentration slows its decrease, and saturates at a small ($\mathcal{O}(\varepsilon)$) size. This stabilization of the monomer concentration is due to the fragmentation of clusters. However, since all other concentrations are $\mathcal{O}(1)$ fragmentation it is still small enough that it does not alter the leading-order concentrations of the clusters; thus they all retain their values from the end of the first timescale.

The third timescale is genuinely slower; fragmentation now affects the leading-order cluster concentrations. Mass is passed from one cluster type to the other by the fragmentation of clusters to monomers which are then used in the growth of clusters of the other type. Clusters now grow to much larger sizes, and consequently the concentration of any particular individual size becomes smaller. Throughout this process the monomer concentration remains $\mathcal{O}(\varepsilon)$, and there is an $\mathcal{O}(1)$ amount of mass to be transferred from one morphology to the other through the monomeric form: thus we expect this timescale to be $t = \mathcal{O}(\varepsilon^{-1})$, as indeed it is. The monomer concentration relaxes to its 'quasi-equilibrium' value on $\mathcal{O}(1)$ timescale, thus can always be assumed to be at this value as given by (3.18). Finally, there is an even longer timescale ($t = \mathcal{O}(\varepsilon^{-2})$) in which all concentrations are small ($\mathcal{O}(\varepsilon)$) and the cluster distribution converges to its equilibrium shape.

3.7. Results from numerical solution of the full system

The full system of equations (3.1) has been solved numerically using a predictor–corrector scheme with timestep h small enough to always satisfy $h \leqslant \varepsilon/10$; simulations for a variety of parameter values have been carried out, and a range of stepsizes were tested to ensure that no numerical artifacts were present in the solution. Results for the case $a = 2.5$, $b = 5$, $\varepsilon = 10^{-2}$, $\varrho = 1$ are presented here. For this choice of parameter, since $a > 1$ we expect clusters of type Y to nucleate in greater abundance initially, but type X to dominate the system at later times since $a < b$. Figure 2 gives three snapshots showing the shape of cluster distributions for both morphologies at the three times $t = 10$, $t = 100$ and $t = 1000$. At $t = 10$, clusters of type Y are seen to dominate ($c_r^Y > c_r^X$) at all aggregation numbers; at time $t = 100$, type X dominates at small sizes ($c_2^X > c_2^Y$ and $c_3^X > c_3^Y$) but at all larger aggregation numbers type Y is still predominant ($c_r^Y > c_r^X$); and by time $t = 1000$, clusters of type X dominate

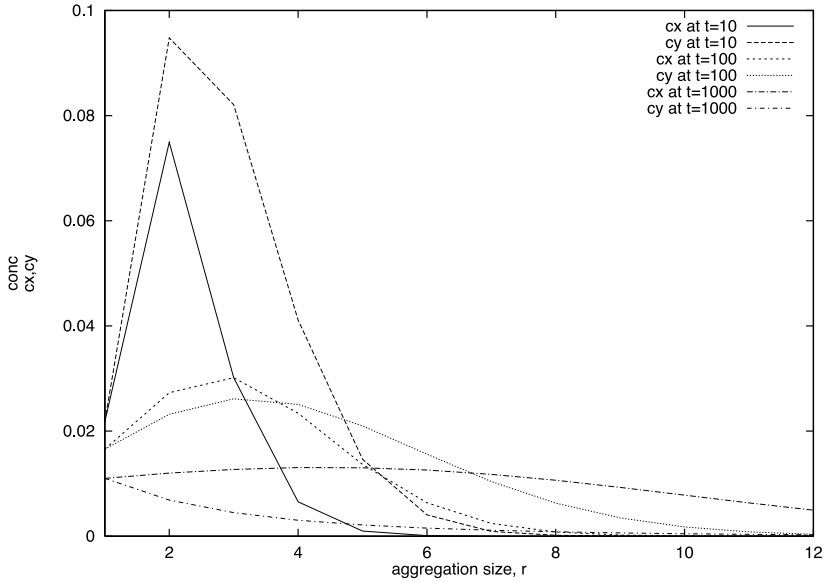

Figure 2. Plots of c_r^X, c_r^Y against r at $t = 10, 100, 1000$ for the case with $a = 2.5$, $b = 5.0$, $\varepsilon = 0.01$, $\rho = 1.0$.

the entire system ($c_r^Y < c_r^X$ for all r). Thus, we observe type Y dominating at small times, due to its larger nucleation rate, but the greater thermodynamic stability of type X becomes evident at later times. Thus, our initial expectations were correct: at intermediate times the greater stability of clusters of type X becomes evident firstly in small clusters and later in larger clusters.

In figure 3 the monomer concentration is shown as a function of time on a log–log plot along with the total number of clusters of each type ($N_X(t)$, $N_Y(t)$) and the mass in each cluster morphology ($\varrho_X(t)$, $\varrho_Y(t)$). The monomer concentration is seen to decay monotonically throughout the process. Initially, all of the variables N_X, N_Y, ϱ_X, ϱ_Y grow and saturate around $t \approx 1$, with $N_Y(t) > N_X(t)$ and $\varrho_Y(t) > \varrho_X(t)$. There then follows a fairly slow evolution of the concentrations; this is the third asymptotic timescale ($t = \mathcal{O}(\varepsilon^{-1})$) over which mass is slowly passed from one morphology to the other. The inequalities cease to be valid after $t \approx 200$, where $N_Y < N_X$ and $\varrho_Y < \varrho_X$. Around this switchover, both N_Y and ϱ_Y decrease, whilst ϱ_X increases and N_X fluctuates without growing much larger. Thus the average size of X-clusters (ϱ_X/N_X) increases in over this timescale. Equilibrium is reached after about $t = 10^4 = \varepsilon^{-2}$ as expected.

Figure 4 is a phase plane plot of ϱ_Y against ϱ_X the trajectory being parametrized by t starting from $\varrho_X = \varrho_Y = 0$ at $t = 0$. In the initial, fast, phase of the nucleation process, $\varrho_X(t)$ and $\varrho_Y(t)$ increase in direct proportion to each other. This ceases at $\varrho_X \approx 0.25$, $\varrho_y \approx 0.7$ where the nonomer concentration has become small ($c_1 = \varrho - \varrho_X - \varrho_Y = \mathcal{O}(\varepsilon)$ where $\varepsilon = 0.01$ and $\varrho = 1$). The trajectory then turns a corner and ϱ_X continues to increase, albeit much more slowly, and now with a corresponding reduction in $\varrho_Y(t)$, until equilibrium is achieved (where $\varrho_X = \varrho - \mathcal{O}(\varepsilon)$ and $\varrho_Y = \varepsilon a(2b - a)/(b - a)$). The trajectory clearly follows closely the line $\varrho_X + \varrho_Y = 1$, the distance below it being the monomer concentration. The dashed curve which remains close to the origin is a plot of N_Y against N_X; this also shows the distinction between the first timescale where both types of cluster grow rapidly, and the later slow timescales where

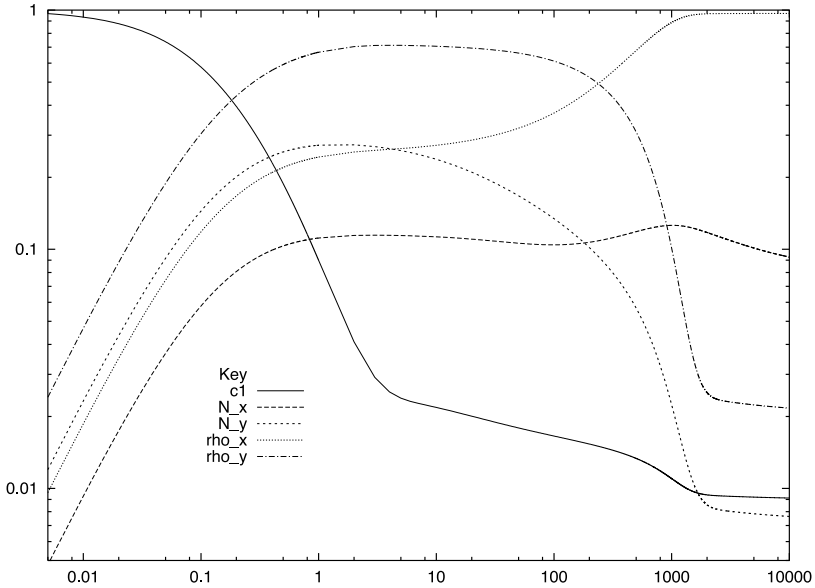

Figure 3. Log–log plots of $N_X, N_Y, \varrho_X, \varrho_Y, c_1$ against t for the case with $a = 2.5$, $b = 5.0$, $\varepsilon = 0.01$, $\rho = 1.0$.

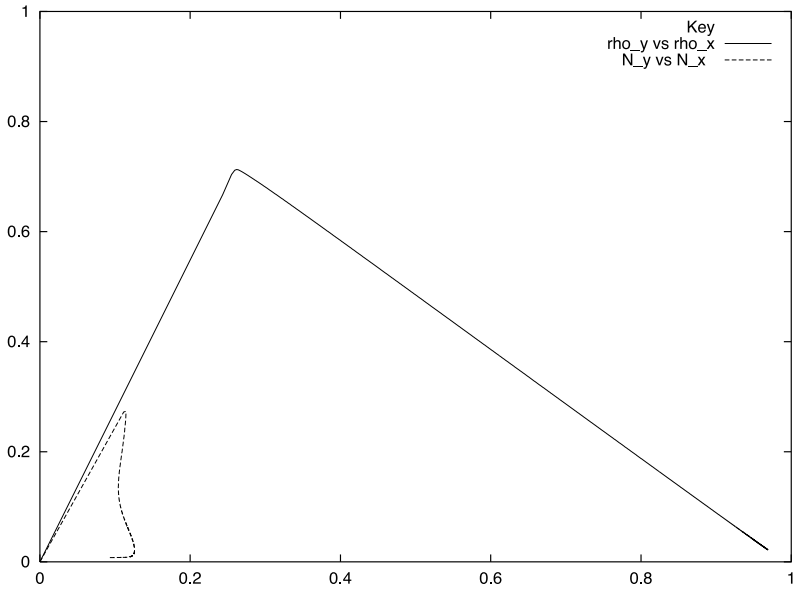

Figure 4. Plots of ϱ_Y against ϱ_X and N_Y against N_X for the case with $a = 2.5$, $b = 5.0$, $\varepsilon = 0.01$, $\rho = 1.0$.

clusters of type Y are broken up to release material for the growing X-clusters. Again we note that in the later stages of the process N_X remains approximately constant and thus the growth in the mass of X-clusters (ϱ_X) is due to a growth in their size.

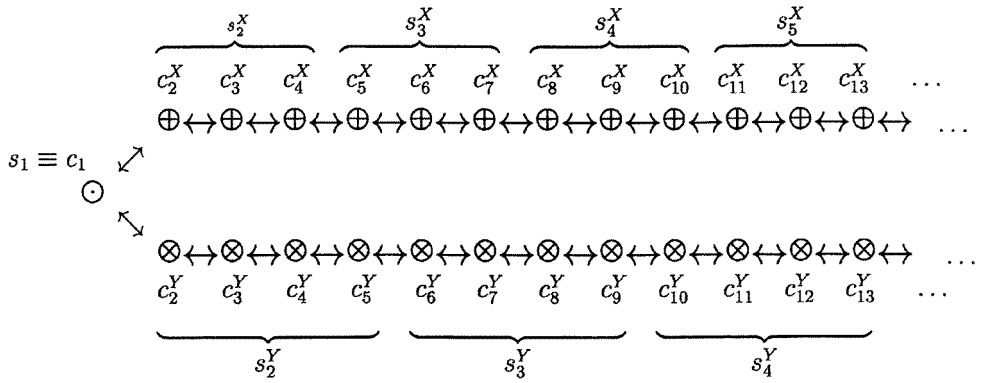

Figure 5. Diagrammatic summary of the coarse-graining contraction applied to the full model of competitive nucleation.

4. Coarse-grained contraction

Equations (2.2) are amenable to a coarse-graining contraction procedure similar to that derived in other generalizations of the Becker–Döring equations [15, 18]. In this case, we define two coarse-grained grids with mesh spacings which may be non-uniform and are allowed to be different for the X- and Y-clusters. We define the mesh for the X-clusters by Λ_n and that for the Y-clusters by Ξ_n. Since the monomer concentration cannot be eliminated from the scheme, we specify $\Lambda_1 = 1 = \Xi_1$. The meshes are then defined by

$$\Lambda_n = (n-1)\lambda + 1 \qquad \Xi_n = (n-1)\xi + 1. \tag{4.1}$$

We eliminate all the concentration variables c_r^X except those which correspond to $r = \Lambda_n$ and eliminate all the c_r^Y except those corresponding to $r = \Xi_n$. We then relabel the retained concentrations by $s_n^X = c_{\Lambda_n}^X$ and $s_n^Y = c_{\Xi_n}^Y$. This procedure, with $\lambda = 3$ and $\xi = 4$, is summarized in figure 5. The monomer concentration in the original formulation (c_1) must be identical to that in the reduced scheme, thus $s_1 \equiv c_1$. The kinetic equations for the new concentrations s_n^X, s_n^Y are then given by

$$\begin{aligned}
&\dot{s}_n^X = L_{n-1}^X - L_n^X \qquad L_n^X = \alpha_n^X s_n^X s_1^\lambda - \beta_{n+1}^X s_{n+1}^X \\
&\dot{s}_n^Y = L_{n-1}^Y - L_n^Y \qquad L_n^Y = \alpha_n^Y s_n^Y s_1^\xi - \beta_{n+1}^Y s_{n+1}^Y \\
&\dot{s}_1 = -\lambda L_1^X - \xi L_1^Y - \sum_{n=1}^{\infty} \lambda^2 L_n^X - \sum_{n=1}^{\infty} \xi^2 L_n^Y
\end{aligned} \tag{4.2}$$

where the constants $\alpha_n^X, \alpha_n^Y, \beta_n^X, \beta_n^Y$ are given by

$$\begin{aligned}
&\alpha_n^X = T^X a_{\Lambda_n}^X a_{\Lambda_n+1}^X \dots a_{\Lambda_{n+1}-1}^X \qquad \beta_{n+1}^X = T^X b_{\Lambda_n+1}^X b_{\Lambda_n+2}^X \dots b_{\Lambda_{n+1}}^X \\
&\alpha_n^Y = T^Y a_{\Xi_n}^Y a_{\Xi_n+1}^Y \dots a_{\Xi_{n+1}-1}^Y \qquad \beta_{n+1}^Y = T^Y b_{\Xi_n+1}^Y b_{\Xi_n+2}^Y \dots b_{\Xi_{n+1}}^Y
\end{aligned} \tag{4.3}$$

and where T^X, T^Y represent constants. In the case of constant coefficients and a uniform mesh, it has been shown in [18] that the optimum choice for the constants T^X, T^Y is

$$T^X = \frac{a^X c_1 - b^X}{\lambda[(a^X)^\lambda c_1^\lambda - (b^X)^\lambda]} \qquad T^Y = \frac{a^Y c_1 - b^Y}{\xi[(a^Y)^\xi c_1^\xi - (b^Y)^\xi]} \tag{4.4}$$

but for an arbitrary mesh and size-dependent rate constants the best choice for T^X, T^Y is not clear.

The system of equations (4.2) can be shown to possess the same properties as the original system; we simply quote the results here:

- A unique equilibrium solution generated from the partition functions Q_r^X, Q_r^Y, namely $\bar{s}_n^X = Q_{\Lambda_n}^X \bar{s}_1^{\Lambda_n}$, $\bar{s}_n^Y = Q_{\Xi_n}^Y \bar{s}_1^{\Xi_n}$. The properties which enable the partition functions to generate an equilibrium solution for the contracted system of equations as well as for the full are

$$\alpha_n^X Q_{\Lambda_n}^X = \beta_{n+1}^X Q_{\Lambda_{n+1}}^X \qquad \alpha_n^Y Q_{\Xi_n}^Y = \beta_{n+1}^Y Q_{\Xi_{n+1}}^Y \tag{4.5}$$

  together with $Q_{\Lambda_1}^X = 1 = Q_{\Xi_1}^Y$.
- A conserved quantity, referred to as the density, $\varrho = s_1 + \sum_{n=2}^{\infty}(\lambda\Lambda_n s_n^X + \xi\Xi_n s_n^Y)$.
- A Lyapunov function, $V = s_1(\log s_1 - 1) + \sum_{n=2}^{\infty}\{\lambda s_n^X(\log(s_n^X/Q_{\Lambda_n}^X) - 1) + \xi s_n^Y(\log(s_n^Y/Q_{\Xi_n}^Y) - 1)\}$.
- A set of identities; for any pair of sequences $\{g_n\}_{n=1}^{\infty}$, $\{h_n\}_{n=1}^{\infty}$ with $g_1 = h_1$

$$g_1\dot{s}_1 + \sum_{n=2}^{\infty}(g_n\dot{s}_n^X + h_n\dot{s}_n^Y) = (g_2 - \lambda(\lambda+1)g_1)L_1^X + (h_2 - \xi(\xi+1)g_1)L_1^Y + \sum_{n=2}^{\infty}(g_{n+1} - g_n - \lambda^2 g_1)L_n^X + \sum_{n=2}^{\infty}(h_{n+1} - h_n - \xi^2 g_1)L_n^Y. \tag{4.6}$$

Thus the coarse-grained contraction has been generalized to construct a mesoscopic or macroscopic model from the original microscopic model derived in section 2.

4.1. Truncated system

In going from the full Becker–Döring system from equations (1.3)–(1.5) to the 'reduced' system (4.2) we have replaced one infinite system of equations by another. It is not until we truncate the system at some finite (but potentially large) aggregation number that we find a gain in efficiency.

There are two natural ways of truncating the normal Becker–Döring system of equations; one method maintains the conservation of density

$$\varrho = \sum_{r=1}^{R} r c_r \tag{4.7}$$

by not allowing clusters larger than size $r = R$ to form. This yields

$$\dot{c}_R = J_{R-1} \tag{4.8}$$

in addition to (1.3)–(1.5) (with (1.3) only holding for $2 \leqslant r \leqslant R-1$) for the system of variables $\{c_r(t)\}_{r=1}^R$. A second truncation method allows the Becker–Döring model of nucleation to be combined with another model for the subsequent growth of clusters. In this model mass can pass out of the 'top' of the system through the formation of clusters of size $r = R+1$; hence, we have

$$\dot{c}_R = J_{R-1} - a_R c_1 c_R + f \tag{4.9}$$

where f represents a source of R-clusters due to the fragmentation of larger clusters as described by another model for clusters of size greater than R. Later, we shall concentrate on the former truncation (4.8) both for simplicity, and because we can confirm that it retains the structure of the Becker–Döring equations: namely, (i) it maintains a conserved quantity (the density $\varrho = \sum_{r=1}^{R} r c_r$) which can be used as a check when carrying out numerical simulations; (ii) it also has a unique equilibrium solution ($c_r = Q_r c_1^r$) generated by the partition function (Q_r); and (iii) a Lyapunov function $V = \sum_{r=1}^{R} c_r(\log(c_r/Q_r) - 1)$.

Provided that λ divides $R-1$, the coarse-grained contraction procedure replaces a system of R equations with a system of $M = 1+(R-1)/\lambda$ equations, where (4.8) or (4.9) is replaced by

$$\dot{x}_M = L_{M-1} \qquad \text{or} \qquad \dot{x}_M = L_{M-1} - \alpha_M x_1^{\lambda} x_M + \phi \tag{4.10}$$

respectively, where ϕ allows the reduced Becker–Döring system to import mass from another model which describes the growth and fragmentation of larger clusters.

In the system generalized for two-component nucleation, let us denote the largest aggregate of type X by R_X and that of type Y by R_Y, then if $(R_X-1)/\lambda = M_X$ and $(R_Y-1)/\xi = M_Y$ the coarse-graining procedure reduces the total system size from R_X+R_Y-1 to M_X+M_Y-1. The choice of the maximum cluster size, and the coarse-graining grid size which is used is arbitrary. The process is an approximation, and choosing small grid sizes will keep errors small; however, later we show that reasonable results can be obtained even with large grid sizes. The benefit of using a coarse-grained model is that there are fewer parameters to be determined. Whereas the full model has R_X+R_Y fluxes and so $2(R_X+R_Y)$ rate parameters to be found, the reduced model has only $2(M_X+M_Y)$. There are many physical effects influencing which grid size is most appropriate in a particular example; in some situations the free energy appears to have quasi-periodic oscillations superimposed on a smooth curve: this provides a natural size scale, as illustrated in figure 2.3 of Lewis [13]. Other mechanisms which may influence the choice of grid size are sizes where inhibition or catalysis becomes important, as discussed in [15, 17].

The generalizations of (4.8) and (4.9) to the two-component system are obvious; for (4.8) it is relatively straightforward to check that the equilibrium solution is $s_r^X = Q^X_{\Lambda_n} s_1^{\Lambda_n}$, $s_r^Y = Q^Y_{\Xi_n} s_1^{\Xi_n}$, where

$$\alpha_n^X Q^X_{\Lambda_n} = \beta^X_{n+1} Q^X_{\Lambda_{n+1}} \qquad \alpha_n^Y Q^Y_{\Xi_n} = \beta^Y_{n+1} Q^Y_{\Xi_{n+1}} \qquad Q_1^X = 1 = Q_1^Y \tag{4.11}$$

and that this equilibrium solution is unique. It can also be verified that the density $\varrho = s_1 + \sum_{n=2}^{M_X} \lambda\Lambda_n s_n^X + \sum_{n=2}^{M_Y} \xi\,\Xi_n s_n^Y$ is conserved, and that

$$V = s_1(\log s_1 - 1) + \sum_{n=2}^{M_X} \lambda s_n^X \left(\log\left(\frac{s_n^X}{Q^X_{\Lambda_n}} \right) - 1 \right) + \sum_{n=2}^{M_Y} \xi s_n^Y \left(\log\left(\frac{s_n^Y}{Q^Y_{\Xi_n}} \right) - 1 \right) \tag{4.12}$$

is a Lyapunov function, and that the system of identities is

$$\begin{aligned} g_1\dot{s}_1 + \sum_{n=2}^{M_X} g_n \dot{s}_n^X + \sum_{n=2}^{M_Y} h_n \dot{s}_n^Y &= (g_2 - \lambda(\lambda+1)g_1)L_1^X + (h_2 - \xi(\xi+1)g_1)L_1^Y \\ &\quad + \sum_{n=2}^{M_X-1} (g_{n+1} - g_n - \lambda^2 g_1) L_n^X + \sum_{n=2}^{M_Y-1} (h_{n+1} - h_n - \xi^2 g_1) L_n^Y. \end{aligned} \tag{4.13}$$

A direct verification of the full model against experiments is not possible due to (i) the large number of unknown rate coefficients, and (ii) difficulties in accurately determining the concentration distribution profile from experimentally data: for example, determining the concentrations of dimers (c_2) as distinct from the concentration of trimers (c_3), etc. However, macroscopic quantities such as those appearing in the model above should be verifiable against experimental results. Since there are potentially very few parameters present in this model, it should be possible to deduce approximate values to them. The system (4.2) is a substantial simplification of the original system, and provides a set of equations which are more amenable to analysis.

4.2. Almost maximally contracted system

As an example of the truncated system described above, let us consider a fairly extreme case where there are only two types of each cluster retained. Thus our model has five concentration variables s_1, s_2^X, s_3^X, s_2^Y and s_3^Y which are determined by

$$\begin{aligned}
\dot{s}_1 &= -\lambda(1+\lambda)L_1^X - \lambda^2 L_2^X - \xi(1+\xi)L_1^Y - \xi^2 L_2^Y \\
\dot{s}_2^X &= L_1^X - L_1^X & L_1^X &= \alpha_1^X s_1^{1+\lambda} - \beta_2^X s_2^X \\
\dot{s}_3^X &= L_2^X & L_1^Y &= \alpha_1^Y s_1^{1+\xi} - \beta_2^Y s_2^Y \\
\dot{s}_2^Y &= L_1^Y - L_2^Y & L_2^X &= \alpha_2^X s_1^{\lambda} s_2^X - \beta_3^X s_3^X \\
\dot{s}_3^Y &= L_2^Y & L_2^Y &= \alpha_2^Y s_1^{\xi} s_2^Y - \beta_3^Y s_3^Y .
\end{aligned} \tag{4.14}$$

This system conserves density:

$$\varrho = s_1 + \lambda(\lambda+1)s_2^X + \lambda(2\lambda+1)s_3^X + \xi(\xi+1)s_2^Y + \xi(2\xi+1)s_3^Y \tag{4.15}$$

and has a Lyapunov function,

$$\begin{aligned}
V = s_1(\log s_1 - 1) &+ \lambda s_2^X \left(\log\left(\frac{\beta_2^X s_2^X}{\alpha_1^X} \right) - 1 \right) + \lambda s_3^X \left(\log\left(\frac{\beta_2^X \beta_3^X s_3^X}{\alpha_1^X \alpha_2^X} \right) - 1 \right) \\
&+ \xi s_2^Y \left(\log\left(\frac{\beta_2^Y s_2^Y}{\alpha_1^Y} \right) - 1 \right) + \xi s_3^Y \left(\log\left(\frac{\beta_2^Y \beta_3^Y s_3^Y}{\alpha_1^Y \alpha_2^Y} \right) - 1 \right).
\end{aligned} \tag{4.16}$$

However, even the examination of this reduced system using analytical techniques is challenging, and requires numerical methods for a detailed analysis. In the next section we shall consider a further simplification, in which only three concentrations are retained.

4.3. Maximally contracted system

We shall now consider ξ, λ large enough such that the system contains just three significant concentrations, namely s_1, s_2^X and s_2^Y, and hence only three equations. Later, this will enable greater analytical progress to be made in the solution of the equations. We now ignore s_r^X, s_r^Y for $r \geqslant 3$, our assumption implying that the amount of these clusters made is negligible: thus we ignore L_r^X, L_r^Y for $r \geqslant 2$. Eliminating all but one concentration of each type of cluster in this way yields

$$\begin{aligned}
\dot{s}_2^X &= \alpha_1^X s_1^{\Lambda} - \beta_2^X s_2^X & \dot{s}_2^Y &= \alpha_1^Y s_1^{\Xi} - \beta_2^Y s_2^Y \\
\dot{s}_1 &= -\lambda\Lambda\alpha_1^X s_1^{\Lambda} + \lambda\Lambda\beta_2^X s_2^X - \xi\,\Xi\alpha_1^Y s_1^{\Xi} + \xi\,\Xi\beta_2^Y s_2^Y
\end{aligned} \tag{4.17}$$

defining $\Lambda = \lambda + 1$, $\Xi = \xi + 1$.

In the next section we apply this model to the coagulation-dominated case analysed earlier, in the original formulation this corresponds to $a_r^X, a_r^Y = \mathcal{O}(1)$ and $b_r^X, b_r^Y = \mathcal{O}(\varepsilon)$. Following the coarse-grained contraction we thus have $\alpha_1^X, \alpha_1^Y = \mathcal{O}(1)$, $\beta_2^X = \mathcal{O}(\varepsilon^{\lambda})$, $\beta_2^Y = \mathcal{O}(\varepsilon^{\xi})$. We thus define $p = \xi/\lambda$, and a new small quantity, $\delta = \mathcal{O}(\varepsilon^{\lambda})$, so that $\varepsilon^{\xi} = \mathcal{O}(\delta^p)$. To simplify ensuing analysis we eliminate all subscripts from the model equations by replacing s_1 by s; s_2^X by u and s_2^Y by v. We work in a timescale such that $\alpha_1^X = 1$, define δ so that $\beta_2^X = \delta$, and then our model can be written as

$$\dot{u} = s^{\Lambda} - \delta u \qquad \dot{v} = \alpha s^{\Xi} - \beta\delta^p v \qquad \dot{s} = \lambda\Lambda\delta u - \lambda\Lambda s^{\Lambda} + \xi\,\Xi\beta\delta^p v - \xi\,\Xi\alpha s^{\Xi} \tag{4.18}$$

for some constants α, β. In practice, the rate constants in the full system of equations are unknown; the rates α, β will be assigned directly into the reduced equations. Thus, we ignore the change of timescale (1.11) since this will automatically be accounted for in the assignment of rates. In the next section we shall show that asymptotic and numerical solutions agree with each other, and provide useful approximations to the kinetics observed in the solution of the full system described in section 3.

5. Analysis of macroscopic model

We have taken the large-λ and large-ξ limit of equations (4.2) so that only one type of cluster of each type need be considered. Due to the possibility of different grain sizes ($\lambda \lessgtr \xi$), there are a number of cases to analyse: $p > 1$, $p < 1$, and $p = 1$. We start by analysing the final case—where the mesh size is the same for clusters of X-type as for Y ($\Lambda = \Xi$), and then move on to the harder problem where $p > 1$. The case $p < 1$ is very similar to $p > 1$ so will not be detailed separately here.

5.1. Equal mesh sizes

Since the system (4.18) has a conserved quantity, $\varrho = s + \Lambda u + \Xi v$, it is further reducible. If we make the two coarse-graining parameters equal ($\Lambda = \lambda + 1 = \Xi$), then the rate equations become

$$\dot{u} = -\delta u + [\varrho - \lambda\Lambda(u+v)]^{\Lambda} \qquad \dot{v} = -\beta\delta v + \alpha[\varrho - \lambda\Lambda(u+v)]^{\Lambda} \tag{5.1}$$

and both occurrences of δ are of the same order of magnitude.

5.1.1. $t = \mathcal{O}(1)$. In the first timescale, both u and v are $\mathcal{O}(1)$ and evolution occurs on the given timescale $t = \mathcal{O}(1)$. The leading-order equations can be solved by noting $\frac{\mathrm{d}v}{\mathrm{d}u} = \alpha$ with $v(0) = 0 = u(0)$ thus $v = \alpha u$, and

$$\begin{aligned} u &= \frac{\varrho}{\lambda\Lambda(1+\alpha)}\left(1 - \frac{1}{[1+\lambda^2\Lambda(1+\alpha)\varrho^{\lambda}t]^{1/\lambda}}\right) \\ v &= \frac{\varrho\alpha}{\lambda\Lambda(1+\alpha)}\left(1 - \frac{1}{[1+\lambda^2\Lambda(1+\alpha)\varrho^{\lambda}t]^{1/\lambda}}\right). \end{aligned} \tag{5.2}$$

Over this first timescale the concentrations of the two species increase in a similar fashion, remaining proportional to each other. As time progresses the rate of increase slows, but the solution is oblivious to the equilibrium configuration, and the fragmentation rates β, δ. The solution ceases to be valid due to the exhaustion of the monomer: new terms enter the leading-order balance when $s = \mathcal{O}(\delta^{1/\Lambda})$. This implies $\varrho - \lambda\Lambda(u+v) \sim \delta^{1/\Lambda}$ which occurs when $t \sim \delta^{-\lambda/\Lambda}$. At this point, a new timescale is necessary.

5.1.2. $t = \mathcal{O}(\delta^{-\lambda/\Lambda})$. Inserting $t = \delta^{-\lambda/\Lambda}t_2$ with $t_2 = \mathcal{O}(1)$ into (5.2), yields

$$\begin{aligned} u &\sim \frac{1}{\lambda\Lambda(1+\alpha)}\left(\varrho - \frac{\delta^{1/\Lambda}}{[\lambda^2\Lambda(1+\alpha)t_2]^{1/\Lambda}}\right) \qquad \text{and} \\ v &\sim \frac{1}{\lambda\Lambda(1+\alpha)}\left(\alpha\varrho - \frac{\delta^{1/\Lambda}\alpha}{[\lambda^2\Lambda(1+\alpha)t_2]^{1/\Lambda}}\right) \qquad \text{as} \quad t_2 \to 0. \end{aligned} \tag{5.3}$$

Thus, we use the new variables u_2, v_2 given by

$$u = \frac{\varrho - \delta^{1/\Lambda}u_2}{\lambda\Lambda(1+\alpha)} \qquad v = \frac{\alpha\varrho - \delta^{1/\Lambda}\alpha v_2}{\lambda\Lambda(1+\alpha)}. \tag{5.4}$$

The equations for $u_2(t_2)$, $v_2(t_2)$ are then

$$\frac{\mathrm{d}u_2}{\mathrm{d}t_2} = \varrho - \frac{\lambda\Lambda(u_2+\alpha v_2)^{\Lambda}}{(1+\alpha)^{\lambda}} \qquad \frac{\mathrm{d}v_2}{\mathrm{d}t_2} = \beta\varrho - \frac{\lambda\Lambda(u_2+\alpha v_2)^{\Lambda}}{(1+\alpha)^{\lambda}}. \tag{5.5}$$

This system can be solved by transforming to the new variables $y_2 = v_2 - u_2$ and $x_2 = u_2 + \alpha v_2$: then the equation for y_2 can be integrated immediately, to $y_2 = (\beta - 1)\varrho t_2$ since at the start of this timescale $y_2 = 0$. The equation for x_2 is

$$\frac{\mathrm{d}x_2}{\mathrm{d}t_2} = \varrho(1+\alpha\beta) - \frac{\lambda\Lambda x_2^{\Lambda}}{(1+\alpha)^{\lambda-1}} \tag{5.6}$$

which cannot be explicitly integrated. By matching with the first timescale we see that $x_2 \sim (1+\alpha)^{\lambda/\Lambda}/(\lambda^2\Lambda t_2)^{1/\Lambda}$ as $t_2 \to 0$. Equation (5.6) shows that x_2 continues to decrease, and asymptotes to $[\varrho(1+\alpha\beta)(1+\alpha)^{\lambda-1}/\lambda\Lambda]^{1/\Lambda}$ as $t_2 \to \infty$.

Over this second timescale the concentrations of the two species diverge linearly with one growing at the expense of the other. This is seen from the growth of y_2 for $\beta > 1$, and decrease if $\beta < 1$. In the former case u increases while v decays, whereas if $\beta < 1$ then y_2 is negative and decreases, giving growth of v and consequent loss of u. These processes occur over a much slower timescale than the initial kinetics.

5.1.3. $t = \mathcal{O}(\delta^{-1})$. The second timescale ceases to be valid due to the increase in y_2. When $t_2 \sim \delta^{-1/\Lambda}$, $y_2 \sim \delta^{-1/\Lambda}$ and another term from the determining equations enters the balance. Thus, in the third timescale we work with $t_3 = \delta t$, $x_3 = x_2$ and $y_3 = \delta^{1/\Lambda} y_2$:

$$\frac{\mathrm{d}y_3}{\mathrm{d}t_3} = \varrho(\beta - 1) - \frac{(\alpha+\beta)y_3}{(1+\alpha)} \tag{5.7}$$

$$0 = \varrho(1+\alpha\beta) + \frac{\alpha(1-\beta)y_3}{(1+\alpha)} - \frac{\lambda\Lambda x_3^{\Lambda}}{(1+\alpha)^{\lambda-1}}. \tag{5.8}$$

The time derivative of x_3 does not appear at leading order, thus x_3 is slaved to y_3. Since equation (5.7) for y_3 is linear, its solution is easily found:

$$y_3 = \frac{\varrho(\beta-1)(1+\alpha)}{(\alpha+\beta)}\left[1 - \exp\left(\frac{-(\alpha+\beta)t_3}{(1+\alpha)}\right)\right]. \tag{5.9}$$

The quantity x_3 can then found from the algebraic equation (5.8). However, x_3 represents a higher-order correction to the concentrations u, v, so does not affect the leading-order results:

$$u = \frac{\varrho}{\lambda\Lambda(1+\alpha)}\left[1 + \frac{\alpha(\beta-1)}{(\alpha+\beta)}\left\{1 - \exp\left(\frac{-t_3(\alpha+\beta)}{(\alpha+1)}\right)\right\}\right] \tag{5.10}$$

$$v = \frac{\varrho\alpha}{\lambda\Lambda(1+\alpha)}\left[1 - \frac{(\beta-1)}{(\alpha+\beta)}\left\{1 - \exp\left(\frac{-t_3(\alpha+\beta)}{(\alpha+1)}\right)\right\}\right]. \tag{5.11}$$

In this solution, the constant of integration has been determined by matching the solution back into the previous timescale, a procedure which shows that as $t_3 \to 0$, $y_3 \sim (\beta-1)\varrho t_3$. The large-time limit behaviour of both the variables u and v is a monotone approach to the constants

$$u \to \frac{\beta\varrho}{\lambda\Lambda(\alpha+\beta)} \qquad v \to \frac{\alpha\varrho}{\lambda\Lambda(\alpha+\beta)} \qquad \text{as} \quad t_3 \to \infty. \tag{5.12}$$

Over this timescale the concentrations approach their equilibrium values on an even slower timescale than the evolution of the second timescale. The complex structure of the approach to equilibrium in the system (5.1) can be seen from the equations themselves. At leading order, a straightforward search for equilibrium states yields a one-parameter family

$$u = \varphi \qquad v = \frac{\varrho}{\lambda\Lambda} - \varphi \qquad \text{for} \quad 0 \leqslant \varphi \leqslant \frac{\varrho}{\lambda\Lambda}. \tag{5.13}$$

This provides the reason for the longer timescales in the above analysis. Over the first timescale the system evolves to one member of this one-parameter family (5.13); then over the second timescale, the trajectory smoothly turns around, and over the third timescale the system moves through this family until it reaches the one member which is a genuine equilibrium solution, i.e. the state which is an equilibrium when all higher-order terms are included (as well as just the leading-order terms).

5.2. Different mesh sizes

The system of equations we aim to solve is (4.18). We now consider the case where $\xi > \lambda$ giving $p = \xi/\lambda > 1$; thus the fragmentation rate of v is much smaller than that of u, leading to an equilibrium configuration in which v dominates u. At equilibrium, to leading order in $\delta \ll 1$, the concentrations take on the values

$$s \sim \left(\frac{\beta\varrho}{\alpha\xi\,\Xi}\right)^{1/\Xi} \delta^{\xi/\lambda\Xi} \qquad u \sim \left(\frac{\beta\varrho}{\alpha\xi\,\Xi}\right)^{\Lambda/\Xi} \delta^{(\xi-\lambda)/\lambda\Xi} \qquad v \sim \frac{\varrho}{\xi\,\Xi}. \tag{5.14}$$

However, at early times, before the effect of fragmentation becomes important, the size of u and v will be comparable, and if $\alpha < 1$ then, at early times, the concentration u will exceed that of v. Thus, at intermediate times we observe concentrations which are wholly unrelated to the equilibrium properties of the system. We now make this argument formal by solving the system (4.18) using matched asymptotic expansions.

5.2.1. $t = \mathcal{O}(1)$. Initially, the system responds on a timescale of $\mathcal{O}(1)$, where all of the concentrations u, v and s take on $\mathcal{O}(1)$ values, with s decaying from ϱ. To leading order, on this timescale, the concentrations evolve according to the equations

$$\dot{u} = s^{\Lambda} \qquad \dot{v} = \alpha s^{\Xi} \qquad \dot{s} = -\lambda\Lambda s^{\Lambda} - \alpha\xi\,\Xi s^{\Xi}. \tag{5.15}$$

Unfortunately, these cannot be solved explicitly, as those in the case $p = 1$ were. But it is possible to determine the large-time asymptotics solutions where $s \to 0$. As $t \to \infty$, $\dot{s} \sim -\lambda\Lambda s^{\Lambda}$ giving $s \sim 1/(\lambda^2\Lambda t)^{1/\lambda}$, $\dot{u} = \mathcal{O}(t^{-\Lambda/\lambda})$ and $\dot{v} = \mathcal{O}(t^{-\Xi/\lambda})$. Thus,

$$u \to u_{1\infty} \qquad \text{and} \qquad v \to v_{1\infty} \qquad \text{as} \quad t \to \infty \tag{5.16}$$

for some constants $u_{1\infty}, v_{1\infty}$. In order to satisfy density conservation, these two constants must satisfy $\varrho = \lambda\Lambda u_{1\infty} + \xi\,\Xi v_{1\infty}$. Thus, over this timescale, both concentrations u and v grow according to the nonlinear equations (5.15), using up, to leading order, all of the available resources of monomer. The decline in monomer concentration is halted by the re-emergence of fragmentation in the limit $t \to \infty$, necessitating the introduction of a new, longer timescale.

5.2.2. $t = \mathcal{O}(\delta^{-\lambda/\Lambda})$. Since $p > 1$, it is the fragmentation term in the u equation in (4.18) which becomes significant first. This occurs when $s^{\Lambda} \sim \delta$, implying $t = \mathcal{O}(\delta^{-\lambda/\Lambda})$. Thus, the new timescale we define is $t_2 = \delta^{\lambda/\Lambda}t$, and over this timescale $s = \delta^{1/\Lambda}s_2$ with $s_2 = \mathcal{O}(1)$. To leading order, the concentrations u and v are $\mathcal{O}(1)$ constants at the end of the first timescale; in the second we allow time-dependent variations around this constant by writing

$$u = u_{1\infty} + \delta^{1/\Lambda}u_2 \qquad v = v_{1\infty} + \delta^{(\Xi-\lambda)/\Lambda}v_2. \tag{5.17}$$

The leading-order equations are then

$$\frac{\mathrm{d}s_2}{\mathrm{d}t_2} = \lambda\Lambda u_{1\infty} - \lambda\Lambda s_2^{\Lambda} \qquad \frac{\mathrm{d}u_2}{\mathrm{d}t_2} = s_2^{\Lambda} - u_{1\infty} \qquad \frac{\mathrm{d}v_2}{\mathrm{d}t_2} = \alpha s_2^{\Xi}. \tag{5.18}$$

Thus, over this timescale, the system tends to the configuration

$$s \to \delta^{1/\Lambda}u_{1\infty}^{1/\Lambda} \qquad u \to u_{1\infty} + \delta^{1/\Lambda}u_{2\infty} \qquad v \to v_{1\infty} + \delta^{\Xi/\Lambda}\alpha u_{1\infty}^{\Xi/\Lambda}t \tag{5.19}$$

for some constant $u_{2\infty}$. The decline in monomer concentration ceases and asymptotes to an $\mathcal{O}(\delta^{1/\Lambda})$ constant. The concentrations u and v undergo minor modifications, with the modification in u tending to a constant, the first correction term in v growing linearly. Since to leading-order all concentrations are constant, and yet the system is not at, or near, equilibrium, further, even longer, timescales are required to analyse the decay of this metastable state, and the genuine approach to equilibrium.

5.2.3. $t = \mathcal{O}(\delta^{-\Xi/\Lambda})$. The growth of the correction term v_2 in (5.19) to the concentration v is unsustainable whilst both of the other concentrations remain constants. At larger times, density conservation will prevent such a solution persisting: in particular, on a timescale of $t = O(\delta^{-\Xi/\Lambda})$. The scalings we now investigate are thus

$$t_3 = \delta^{\Xi/\Lambda} t \qquad s = \delta^{1/\Lambda} s_3(t_3) \qquad u = u_3(t_3) = \mathcal{O}(1) \qquad v = v_3(t_3) = \mathcal{O}(1). \tag{5.20}$$

The leading-order determining equations are

$$\varrho = \lambda\Lambda u_3 + \xi\,\Xi v_3 \qquad 0 = s_4^{\Lambda} - u_4 \qquad \frac{\mathrm{d}v_4}{\mathrm{d}t_4} = \alpha s_4^{\Xi} \tag{5.21}$$

where the equation for conservation of density has been used in place of the differential equation for s. These can be rearranged to show that u_3 satisfies $\mathrm{d}u_3/\mathrm{d}t_3 = -\xi\,\Xi\alpha u_3^{\Xi/\Lambda}/\lambda\Lambda$, which is solved by

$$u_3 = \frac{1}{[u_{1\infty}^{-(\Xi-\Lambda)/\Lambda} + \alpha\xi\,\Xi(\Xi-\Lambda)t_3/\lambda\Lambda^2]^{\Lambda/(\Xi-\Lambda)}} \tag{5.22}$$

with the solutions for v_3, s_3 following immediately by

$$s_3 = u_3^{1/\Lambda} \qquad v_3 = \frac{\varrho - \lambda\Lambda u_3}{\xi\,\Xi}. \tag{5.23}$$

This solution describes the relaxation of the metastable state since it is over this timescale that the concentration u decays from being of $\mathcal{O}(1)$ to being small. During this timescale, the cluster concentration u is in equilibrium with the monomer concentration s. However, monomers are continually combining to increase the concentration of the v-morphology, causing u and s to decrease monotonically. At large times the above solution ceases to be valid, since the decay of u is accompanied by a decay in the monomer concentration (s), and when $s = \mathcal{O}(\delta^{\xi/\lambda\Xi})$ the fragmentation of v becomes significant.

5.2.4. $t = \mathcal{O}(\delta^{-(p\xi+1)/\Xi})$. At the end of the previous timescale, (5.22) and (5.23) imply that $v \to \varrho/\Xi$; thus v reaches its leading-order equilibrium value at the end of the previous timescale and only undergoes small modifications in this fourth timescale. The fragmentation of v becomes relevant when $t_3 = \mathcal{O}(\delta^{-(\Xi-\Lambda)^2/\lambda\Lambda})$, which implies that the new timescale is determined by $t = \delta^{-(p\xi+1)/\Xi} t_4$ with $t_4 = \mathcal{O}(1)$. On this timescale $s = \delta^{p/\Xi} s_4$, $u = \delta^{(p-1)/\Xi} u_4$ and $v = \varrho/\xi\,\Xi - \delta^{(p-1)/\Xi} v_4$. The leading-order equations for these quantities are then

$$0 = \lambda\Lambda u_4 - \xi\,\Xi v_4 \qquad -\frac{\mathrm{d}v_4}{\mathrm{d}t_4} = \alpha s_4^{\Xi} - \frac{\beta\varrho}{\xi\,\Xi} \qquad 0 = s_4^{\Lambda} - u_4. \tag{5.24}$$

Here the monomers (with concentration s) equilibrate with the dominant cluster morphology (v) through a term representing the fragmentation of v-clusters, the first time β has entered our analysis. The system (5.24) is solved by

$$t_4 = \int_{\frac{\xi\Xi v_4}{\lambda\Lambda}}^{\infty} \frac{\lambda\Lambda\,\mathrm{d}x}{\alpha\xi\,\Xi x^{\Xi/\Lambda} - \beta\varrho} \qquad u_4 = \frac{\xi\,\Xi v_4}{\lambda\Lambda} \qquad s_4 = u_4^{1/\Lambda}. \tag{5.25}$$

Over this timescale, the solution reaches equilibrium since the leading-order large-time asymptotics of this solution agree with the previously described equilibrium solution (5.14).

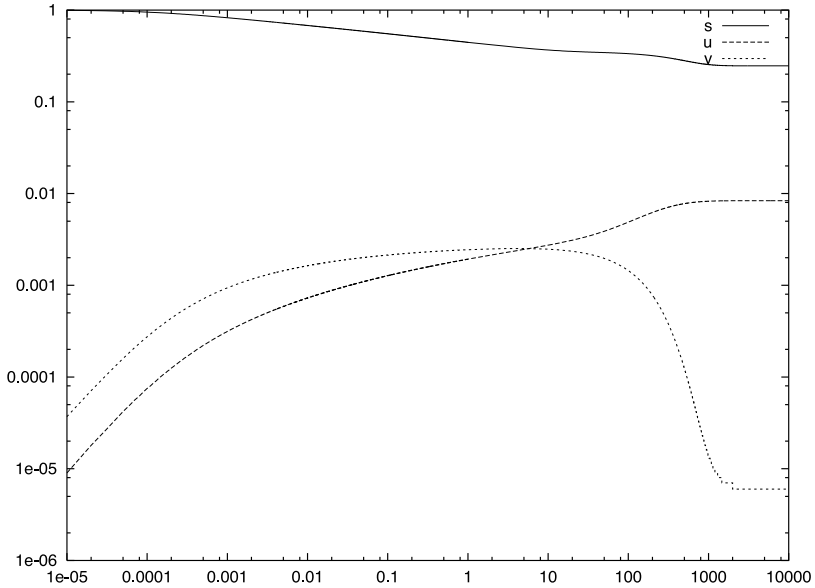

Figure 6. Plots of s, u, v against t for the maximally contracted case with $\alpha = 4$, $\beta = 8$, $\delta = 0.0001$, $\rho = 1.0$, $\lambda = 9$, $\xi = 12$.

5.3. Results from numerical solution of the reduced system

The maximally contracted system of equations (4.18) has been solved numerically (again using a predictor–corrector scheme with timestep $h < \delta/10$), and results for the case $\alpha = 4$, $\beta = 8$, $\delta = 10^{-4}$, $\lambda = 9$, $\xi = 12$, $\varrho = 1$ are presented here. Figure 6 shows a log–log plot of the concentrations of the two cluster types and the monomer source against time. The initial growth of both cluster types is seen to slow as the monomer becomes exhausted, and the eventual overtaking of $v(t)$ by $u(t)$ occurs at $t \approx 5$; after this the concentration u continues to increase at the expense of v, through the fragmentation of v to monomers and subsequent aggregation of monomer to form more larger clusters of type u. Figure 6 should be compared with figure 3, where we observe a qualitatively similar shape of curves. The differences in amplitude of the monomer concentration are due to the fact that δ was only taken to be 10^{-4}, whereas a full comparison with the example shown in figure 3 would require $\delta = \varepsilon^{\lambda} = 10^{-18}$. There are considerable problems in the numerical solution of systems with such small parameters, hence such an extreme case was not attempted here.

Figure 7 shows a trajectory in (u, v) phase space: $t = 0$ corresponds to the origin $\varrho_X = 0 = \varrho_Y$, both cluster types form, and a maximum in v occurs when $u \approx 0.0025$. At this point the slow timescales are entered, and the system then slowly evolves down the diagonal straight line, the monomer concentration being uniformly small from this point until equilibrium is achieved, where v is almost zero. This figure is analogous to figure 4 which represents data from a numerical solution of the full problem.

The asymptotic results enable this behaviour to be described as occurring over four timescales: over the first both cluster types grow and exhaust the supply of monomer. Over the second, longer, timescale, fragmentation causes the monomer concentration to stabilize at some small positive constant. During the third, even longer, timescale the monomer concentration remains small while fragmentation now influences the cluster concentrations, causing mass to pass from one less thermodynamically stable morphology to the more stable form. Finally,

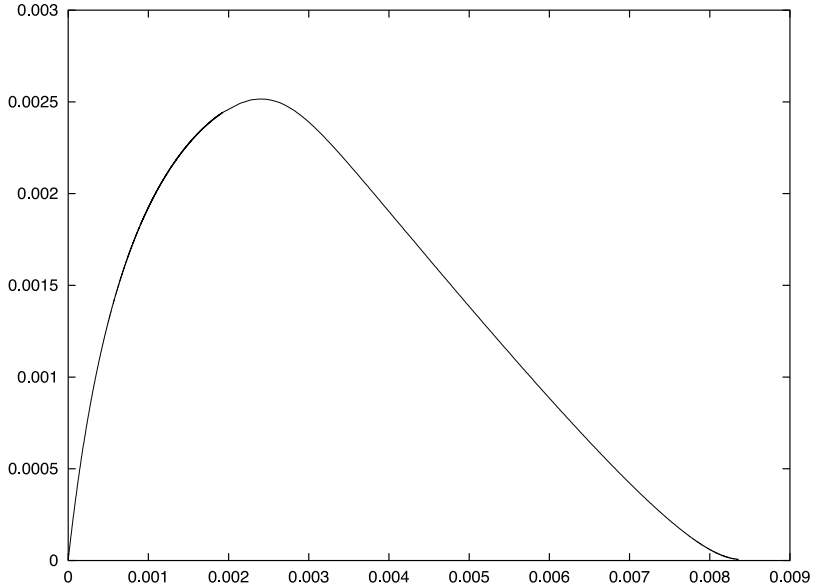

Figure 7. Plots of v against u for the maximally contracted case with $\alpha = 4$, $\beta = 8$, $\delta = 0.0001$, $\rho = 1.0$, $\lambda = 9$, $\xi = 12$.

there is an even longer timescale over which equilibrium is reached, at equilibrium almost all the mass is in one form, there being only asymptotically small amounts of monomer and of the less stable cluster morphology.

6. Discussion

We have proposed a model for nucleation in which two morphologies of cluster are able to form from a single type of monomer. Clusters of both structures grow according to classical nucleation theory and, if we were to impose a constant monomer concentration then the growth of each cluster-type would be independent of each other. However, we have considered the more relevant and interesting case where the total concentration of material is kept constant: this means that the two species of cluster compete for the finite amount of monomeric material present within the system, and the relative growth rates of the two types of cluster then become important in the kinetics of nucleation. By considering an aggregation-dominated system we have been able to determine the form of the solution through the use of matched asymptotic expansions. The structure of the solution has been found in the special case where all aggregation and fragmentation rates are independent of cluster size.

Asymptotic analysis of the full model identifies a sequence of four timescales over which the kinetics occur. The complexity of the problem precluded a full explicit form for the cluster-distribution function being found, but approximations were derived in the matching regions. During the first timescale fragmentation is negligible and sizable concentrations of both types of cluster are formed, typically having small aggregation numbers. The number of clusters formed depends solely on the aggregation rate, and not on the thermodynamic stability of the clusters. The monomers are rapidly used up, and over a second timescale the monomer concentration becomes, and stays small. During the third timescale, which is a slow timescale, mass is transferred from the less thermodynamically stable to the more stable form through

the fragmentation of the less stable clusters into monomers and the growth in size of the more stable form of cluster. However, equilibrium is not reached over this timescale, since the cluster-distribution function is given by a similarity solution and is constantly evolving. Finally, over a fourth, even slower timescale, the system reaches its equilibrium configuration. Over this timescale the distribution function for the more stable form satisfies a continuum version of the Becker–Döring equations. The special case where the two morphologies are equally stable has been analysed, and results are broadly similar to the general case, though they cannot be obtained directly from it. The system of equations was then solved numerically and for one choice of parameters the results were presented. The sequence of behaviour over the timescales described above is seen in the numerical results also, confirming the validity of the asymptotic expansions.

A coarse-graining contraction procedure was invoked and used to simplify the equations by reducing the dimensionality of the system. When applied to a truncated version of our modified Becker–Döring equations, a system of just three ordinary differential equations was ultimately obtained. The simplified system was solved using matched asymptotic analysis in two cases. In the first, the mesh size (or grain size) was taken to be the same for both species of cluster. This gave kinetics which occurred on three timescales, an initial growth in both morphologies, followed by a long timescale during which the concentrations changed linearly, and a final slightly longer timescale over which the concentrations underwent slight modifications to equilibrium. In the second case, the mesh sizes for the two species are taken to be different. This leads to a situation in which one species dominates the other at equilibrium. The kinetics in this case are more complex, there being four timescales through which the system evolves. Initially, the species with the faster aggregation rate gains the larger concentration, regardless of which is more thermodynamically stable. Although this may appear obvious at the start of the reaction, the system passes through a long timescale before the final equilibrium form of the solution starts to influence the kinetics of the reaction. This sequence of events can also be clearly identified in the numerical solution of the equations. If clusters of the more stable morphology have a smaller growth rate than clusters of the less stable form then the less stable clusters will gain a greater concentration initially, and then such a state will persist until the penultimate timescale—a surprisingly long time. The system can thus be viewed as entering a metastable state in which the concentrations of both forms of cluster are comparably large, and the monomer concentration is small. In this state no concentration is near its final equilibrium value, yet evolution occurs on a slow timescale due to the low concentration of monomers.

Thus we have elucidated some of the reasons for metastability in the process of nucleation by considering a system in which two morphologies of solid can precipitate out from a supersaturated solution or supercooled melt. Although inspired from classical nucleation theory, our model does not require the solids to be crystalline: they could be gels, or amorphous solids; such information would only affect the coagulation and fragmentation rate coefficients, but not the form of the equations. A good example of such a system, in which two cluster types can be formed from a single monomer type, are the chiral crystallization experiments conducted by Kondepudi *et al* [10–12]. In these, an achiral monomer can nucleate to form one of two types of crystal, namely a left- and a right-handed product. An explanation of the effects investigated by Kondepudi *et al* requires secondary nucleation to be included in our model (in the manner of [15]), and so falls beyond the scope of the current work but, in a future work, it is hoped to generalize the model presented here to include nucleation by both primary (homogeneous) and secondary means and present an investigation into the resulting system of equations.

Acknowledgments

I would like to thank both Professor John King and Professor Peter Coveney for many useful discussions. I am grateful to the University of Nottingham for assistance under their scheme for new lecturers.

References

[1] Allcock H R and Lampe F W 1981 *Contemporary Polymer Chemistry* (New Jersey: Prentice-Hall) ch 12
[2] Aniansson G E A and Wall S N 1974 On the step-wise micelle association *J. Phys. Chem.* **78** 1024–30
[3] Becker R and Döring W 1935 Kinetische behandlung der keimbildung in ubersattigten dampfern *Ann. Phys.* **24** 719–52
[4] Brilliantov N V and Kravitsky P L 1991 Non-scaling and source-induced scaling behaviour in aggregation models of movable monomers and immovable clusters *J. Phys. A: Math. Gen.* **24** 4787–803
[5] Coveney P V and Wattis J A D 1996 Analysis of a generalized Becker–Döring model of self-reproducing micelles *Proc. R. Soc.* **452** 2079–102
[6] Coveney P V and Wattis J A D 1998 A Becker–Döring model of autopoietic self-reproducing vesicles *J. Chem. Soc.: Faraday Trans.* **102** 233–46
[7] Coveney P V and Wattis J A D 1999 Cluster renormalization in the Becker–Döring equations *J. Phys. A: Math. Gen.* **32** 7145–52
[8] Kam Z, Shore H B and Feher G 1978 On the crystallization of proteins *J. Mol. Biol.* **123** 539–55
[9] Keller A, Goldbeck-Wood G and Hikosaka M 1993 Polymer crystallization: survey and new trends with wider implications for phase transformations *Faraday Discuss.* **95** 109–28
[10] Kondepudi D K, Kaufman R J and Singh N 1990 Chiral symmetry breaking in sodium chlorate crystallization *Science* **250** 975–6
[11] Kondepudi D K, Bullock K L, Digits J A, Hall J K and Miller J M 1993 Kinetics of chiral symmetry breaking in crystallization *J. Am. Chem. Soc.* **115** 10 211–16
[12] Kondepudi D K, Bullock K L, Digits J A and Yarborough P D 1995 Stirring rate as a critical parameter in chiral symmetry breaking crystallization *J. Am. Chem. Soc.* **117** 401–4
[13] Lewis B 1975 Nucleation and growth theory Crystal Growth ed B R Pamplin (Oxford: Pergamon Press) ch 2 pp 12–39
[14] Toschev S 1973 *Crystal Growth: An Introduction* ed P Hartman (Amsterdam: North-Holland)
[15] Wattis J A D and Coveney P V 1997 General nucleation theory with inhibition for chemically reacting systems *J. Chem. Phys.* **106** 9122–40
[16] Wattis J A D and Coveney P V 1999 The origin of the RNA world: a kinetic model *J. Phys. Chem.* **103** 4231–50
[17] Wattis J A D and Coveney P V 1999 Models of nucleation and growth mechanisms: the challenge to experiment *PCCP* **1** 2163–76
[18] Wattis J A D and King J R 1998 Asymptotic solutions of the Becker–Döring equations *J. Phys. A: Math. Gen.* **31** 7169–89